June 1991 Research Report UMCE 91-14

OPTIMUM DESIGN OF EARTHQUAKE RESISTANT MODULAR STRUCTURES

Hossein E. Keshtkar
Robert D. Hanson
Richard A. Scott

Department of Civil Engineering
The University of Michigan
College of Engineering
Ann Arbor, MI 48109-2125

eng

UMR0384

ACKNOWLEDGMENTS

Professors Subhash C. Goel and James K. Wight reviewed the manuscript. Their comments and suggestions are gratefully acknowledged.

TABLE OF CONTENTS

LIST OF FIGURES

LIST OF TABLES

CHAPTER 1

SEISMIC DESIGN AND MODULAR STRUCTURES

1.1 Introduction

The ancient Japanese wooden pagodas have survived repeated earthquakes for centuries without any serious structural damage. Tanabashi (1960) attributes this superb performance to the flexibility and the large inherent damping of the wooden pagodas. The fundamental period of these structures is longer than the dominant period of Japanese earthquakes and thus the transfer of energy is limited to tolerable amounts. Moreover, the laminated timber construction of the beams and the overhangs provides a medium of effective frictional damping which alleviates the damaging deformations that would otherwise take place in the event of an earthquake. These ancient temples, with regard to their flexibility and large damping, are functional and tested examples of the innovative ideas underlying the concepts of base isolation and supplemental damping in modern multistory building structures.

The elastic response of conventional buildings to earthquake motion is primarily influenced by the mass, stiffness, and damping properties of the structural framework. The minimum amount and distribution of mass along the height of the building is predetermined in the process of design for gravity. The additional mass due to the lateral force design, especially in steel structures, is insignificant. A minimum lateral stiffness is required to limit interstory drift for protection of nonstructural elements. The damping characteristic is difficult to evaluate. Its amount, in the elastic range, is small and varies little from one type of structure to another.

The fundamental periods of most low to medium rise conventional buildings fall in the range of the dominant periods of earthquakes recorded on rock or competent soil. To improve the elastic response for such structures, the mass, stiffness, and damping properties have to be changed. The mass and stiffness, as just mentioned, have fixed minimum values due to structural design for gravity and interstory drift limits. Adding nonstructural mass for the sake of response improvement is economically

undesirable; and an increase in lateral stiffness will add cost, if not considerable mass, and will limit open space that is of high priority in most modern buildings. With these restrictions, and given that the inherent damping in the elastic range is small, the low to medium rise conventional building has a predetermined fate as far as its response to intense earthquakes is concerned; that is, the response will reach and go beyond the elastic limit.

As the conventional structure deforms plastically in an intense earthquake, there will be a considerable dissipation of the imparted energy. This is the contention of the traditional philosophy of design for large earthquakes. Based on this philosophy, the connections, beams, braces, columns, and shear walls are so designed as to behave in a ductile manner under repeated hysteretic deformations while preventing collapse of the structure. Structural damage is therefore permitted in this method of earthquake resistant design (Newmark and Rosenblueth, 1971). The philosophy is not to avoid but to resist the violent shaking of the ground in an intense earthquake.

In the concept of base isolation the intention is to avoid the high energy content of the earthquake by lengthening the period of the structure (Kelly, 1986). This is achieved by erecting the building on soft springs, commonly called isolators, which are capable of sustaining large lateral deformations. Most of the deformation takes place locally at the base, and the superstructure incurs minimal lateral force levels and stays elastic. The level of the superstructure's response improvement therefore depends on the lateral flexibility of the isolators. Of course, the isolators should have the capability to hold the weight of the building, restore the building to its original position after earthquake is diminished, and be very stiff vertically so that large vertical and rocking motions of the building are prevented. In order to limit intolerable displacements of the isolators, some damping mechanism is also incorporated at the isolator level (Kelly and Beucke, 1983).

The method of providing supplemental damping within the framework of a structure is fundamentally the same as invoking the inherent hysteretic damping of the conventional building. In this method, however, the novelty is that the source and the location of energy dissipation, for the most part, is localized within energy absorbing devices which link various parts of the framing system (Bergman and Hanson, 1988; Kelly and Skinner, 1979).

In this research the ideas underlying the base isolation and supplemental damping are incorporated in a more general structural system, here referred to as a *modular structure*. This system is particularly well adopted to a mathematical model in which damping and stiffness properties can vary with substantial freedom to facilitate opti-

mization of its elastic response to earthquakes.

1.2 Description of a Modular Structure

The schematic of a three-story modular structure is shown in Fig. 1.1. In this two-dimensional frame, one floor beam, two columns, one chevron brace, and one diaphragm beam constitute the design of all three similar *modules*. The roof is also considered as an independent module. Every module is separated from a neighboring one by means of two *control elements*. A control element represents a combination of a lateral spring and a damper. The diaphragm beam is primarily meant to transfer the lateral load to the chevron brace which, in this case, provides the lateral load resisting mechanism.

In a three dimensional multi bay extension of this structural framework, the chevron braces will be required only at a limited number of bays in each direction. The diaphragm beams, however, must be present at every bay in order to rigidly connect the top ends of neighboring columns in a grillage pattern. Further bracing in the plane of this grillage may also be required to provide an adequate diaphragm action. The grillage system is therefore a source of additional weight which must be carried by the columns and the braces to the foundation. This additional weight, however, is small compared to the weight of the floor system which carries all of the floor dead and live loads.

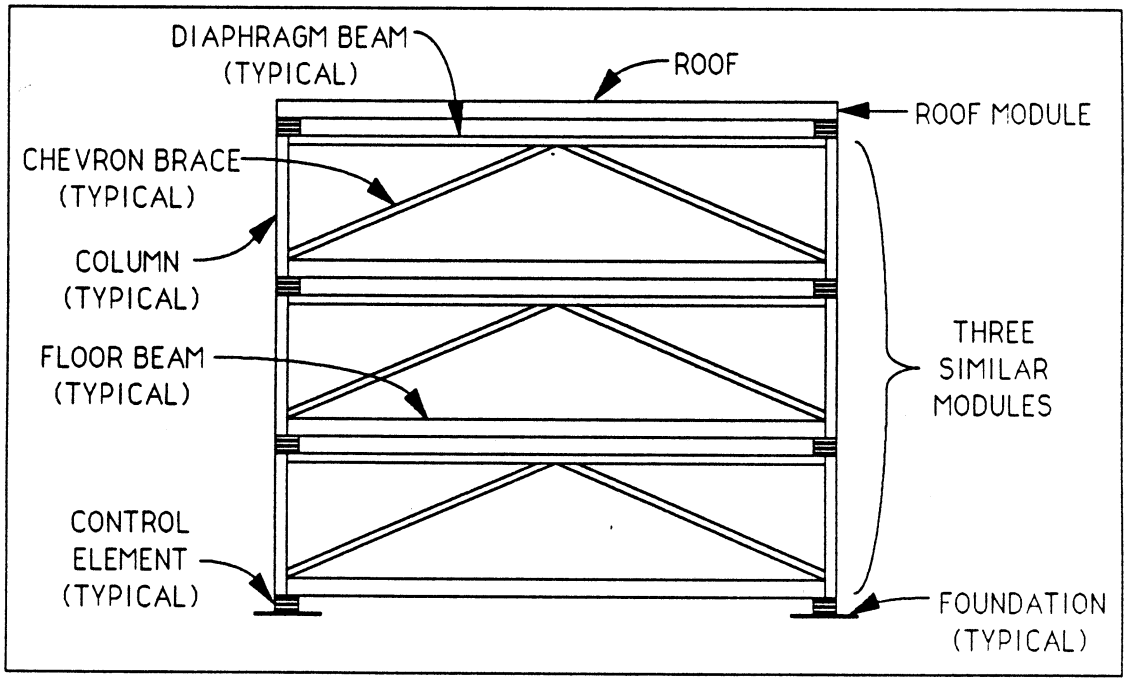

Fig. 1.1 *Schematic of a three-story modular structure*

In the illustrative model presented in Fig. 1.1, the control elements are located at all four possible levels. Other modular models can also be produced by choosing fewer levels of control elements. For instance, Fig. 1.2 shows a model in which the control elements are placed at the base and between the second and third stories. In this case, the first two stories are taken as the first module and the third floor, including the roof, as the second.

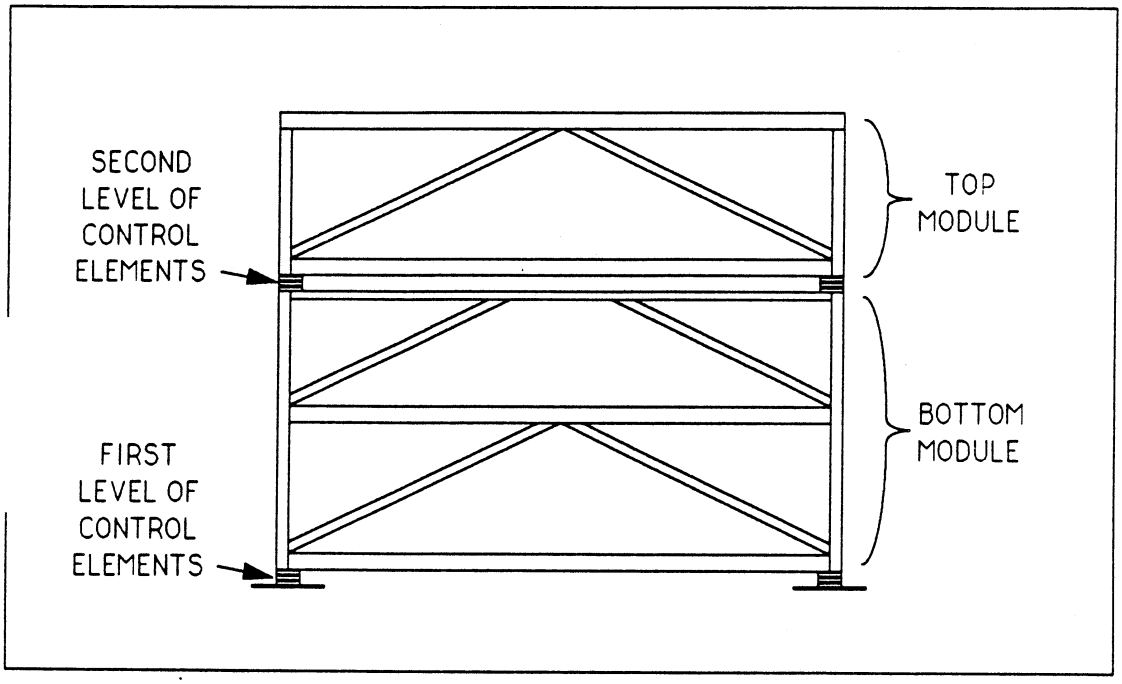

Fig. 1.2 *A three-story modular structure with two levels of control elements*

A control element is similar to currently used base isolators. Lin, Tadjbakhsh, Papageorgiou, and Ahmadi (1990) have described the mechanisms of various isolation systems and conducted a comparative study of their performance in buildings subjected to strong earthquakes. Ideally, a control element should be capable of providing low lateral stiffness, high vertical stiffness, and some degree of damping. One type of control element, commonly used in base isolation applications, is composed of laminated rubber and reinforcing steel layers. This system will be described in Section 1.4 in order to provide a basis for choosing practical constraints on the optimal design of modular structures.

In a modular structure subjected to earthquake motion, *intermodule* displacements are expected to reach several inches. This requires special design considerations for the elevators, stairs, plumbing, ductwork, and wiring. With the exception of elevators, the rest require only slight modifications. The stairs are integral parts of the modules

and should simply have discontinuities at the control element levels. Plumbing in the control element region can be of flexible material, such as copper, coiled in several pitches, and securely anchored to the neighboring modules. The segments of duct work which pass through the control element region can be made of durable fabrics with sufficient sag for relative movements of the sheet metal parts. All wiring should be simply sagged at the control element levels. Special design considerations for the elevators require that the elevator shaft be large enough to allow for the predicted motion of the modules. In this case the gap between the entrance to the elevator cab and the cab floor can be closed by a variety of seismic joints whose details are beyond the present discussion.

To protect nonstructural elements, the individual modules can be designed for any level of lateral stiffness irrespective of the stiffness of the control elements. The bracing system shown in Fig. 1.1 serves as an illustration. Any lateral load resisting mechanism, including concrete or steel moment frames or shear walls, can be used. It is reasonable to expect that the lateral stiffness of the modules will be much larger than the lateral stiffness of the control elements, so that in a preliminary design cycle the characteristics of the system stiffness matrix can be based solely upon the stiffness of the control elements. Ignoring the small inherent damping in the modules, the system damping matrix can be drawn completely from the measurable damping properties of the control elements. These features provide a simple mathematical model for the dynamic behavior of the modular structure. For instance, the three-story modular structure of Fig. 1.1 behaves like a simply coupled four degree of freedom system with a diagonal mass matrix and symmetric tridiagonal damping and stiffness matrices.

From the foregoing description it is evident that the construction of a modular structure may be more costly than that of a conventional one. This is in part due to the need for additional structural systems, such as the diaphragms and the control elements; and in part due to the special design requirements for the various service components of the building, such as the elevators and the stairs. The advantage of tolerating the additional cost is the enhanced control over the dynamical performance of the structure subjected to a prescribed ground motion. When the control elements are allowed at every possible level within the structure, a maximum level of control is achieved since the number of control parameters of the problem is at a maximum. On the other hand, fewer levels of control elements limit the control over performance but also reduce the total construction cost of the building.

A base isolated structure is a special form of a modular structure in which the control elements are placed only at the base. It is also of interest to note that placement of the control elements at the base and at one other location between adjacent stories will create a classic case of vibration isolation. Vibration isolation utilizing a tuned mass damper has been traditionally applied to reduction of wind induced vibrations in tall buildings (McNamara, 1977). The effect of tuned mass dampers on seismic response of structures has been studied by Slasek and Klingner (1983) who concluded that no reduction in lateral forces can be achieved. This conclusion is entirely due to the practical limit that they placed on the mass of the tuned mass damper. Kaynia, Veneziano, and Biggs (1981) conducted a more extensive investigation of the same problem and arrived at a similar conclusion for tuned mass dampers of small mass.

In a two degree of freedom modular model, the top module and the connecting control elements can be regarded as a tuned mass damper for the bottom module. In this sense the restriction of a practical level of mass for the tuned mass damper does not apply and substantial response improvements can be achieved. Curtis and Boykin (1961) and Crandall and Mark (1963) performed extensive parametric studies of a two degree of freedom system subjected to white noise base excitation. They investigated the vibration absorber action of the second mass and concluded that indeed the possibility of vibration isolation exists for sufficiently large magnitude of the second mass. This is practically possible in a modular structure.

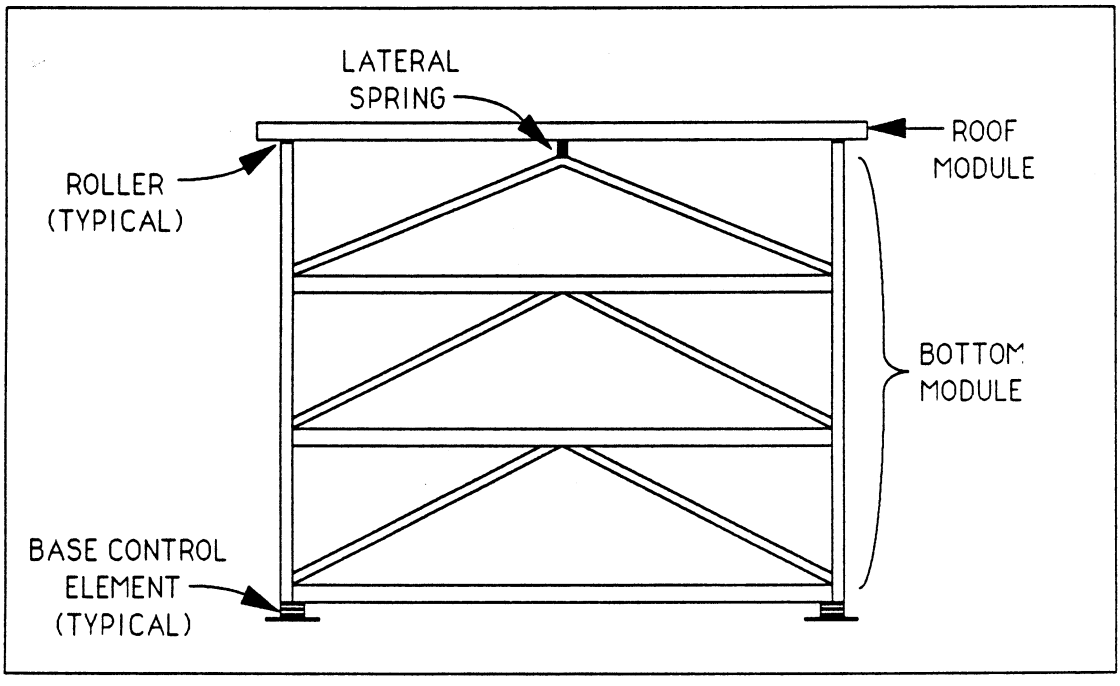

Fig. 1.3 *Separation of vertical and lateral supports at the roof level*

Of particular interest is a two degree of freedom modular model with the control elements placed at the base and just under the roof. In this case, because of the relatively small weight of the roof, the supporting control elements can be divided into two distinctly different mechanisms. A possible detail for a two dimensional frame is shown in Fig. 1.3 in which the entire vertical roof load is transferred to the cantilever columns through rollers; and the lateral load is transferred to a chevron brace by means of a lateral spring. The rollers, for instance, can represent polished and lubricated overlapping surfaces of steel plates; and the lateral spring can be a vertically positioned helical spring or a stub column made of rubber with no reinforcing steel plates. In this design, since the lateral load taken by the columns is minimal, a diaphragm beam is no longer necessary. Moreover, the number of lateral springs required will be equal to the number of chevron braces used. With some additional bracing details, this idea can be extended to three dimensional multi bay frames.

1.3 A Six-Story Building Example

A potential candidate for a modular scheme is a low to medium rise building whose height and plan dimensions have the same order of magnitude. A six-story steel building shown in Fig. 1.4 satisfies this requirement. Various two degree of freedom *(2dof)* models of this building will be used in Chapter 3 in the investigation of the optimal design. Each model requires two levels of control elements. The first level is always placed at the base of the building and the second level at one of the six possible locations as indicated in Fig. 1.4a. With this arrangement, there are six *2dof* models with different modular mass distributions.

With reference to Fig. 1.4b, the selected floor plan utilizes a total of 24 columns. It is assumed that the number of control elements at each level is also 24, each placed directly under one column. It is further assumed that the control elements at one level have the same lateral properties. Under these circumstances, the mass, stiffness, and damping of the *2dof* models are equivalently taken as one twenty fourth of the actual values.

In order to avoid unrealistic mass distributions in the models, it is necessary to make a rough estimate of the weight of various building components which contribute to dead load. These, under separate headings for the floors and the roof, are listed in Table 1.1 in terms of the pound per square foot *(psf)* of the plan area. The dead loads for the floors and the roof are listed in the last row as the sum of the individual components. Referring to Fig. 1.4b, one twenty fourth of the plan area is

approximately 542 ft^2. With this value and the aid of Table 1.1, the floor and roof dead loads, for the equivalent models, can be computed as

$$\begin{aligned} \text{floor dead load} &\simeq 50\ kips \\ \text{roof dead load} &\simeq 50\ kips \end{aligned}$$

Table 1.2 summarizes the weight distribution for the six *2dof* equivalent modular models. In the last row, the 7th model corresponds to the base isolated version. These models will be used in the optimal design studies which will be pursued in Chapter 3.

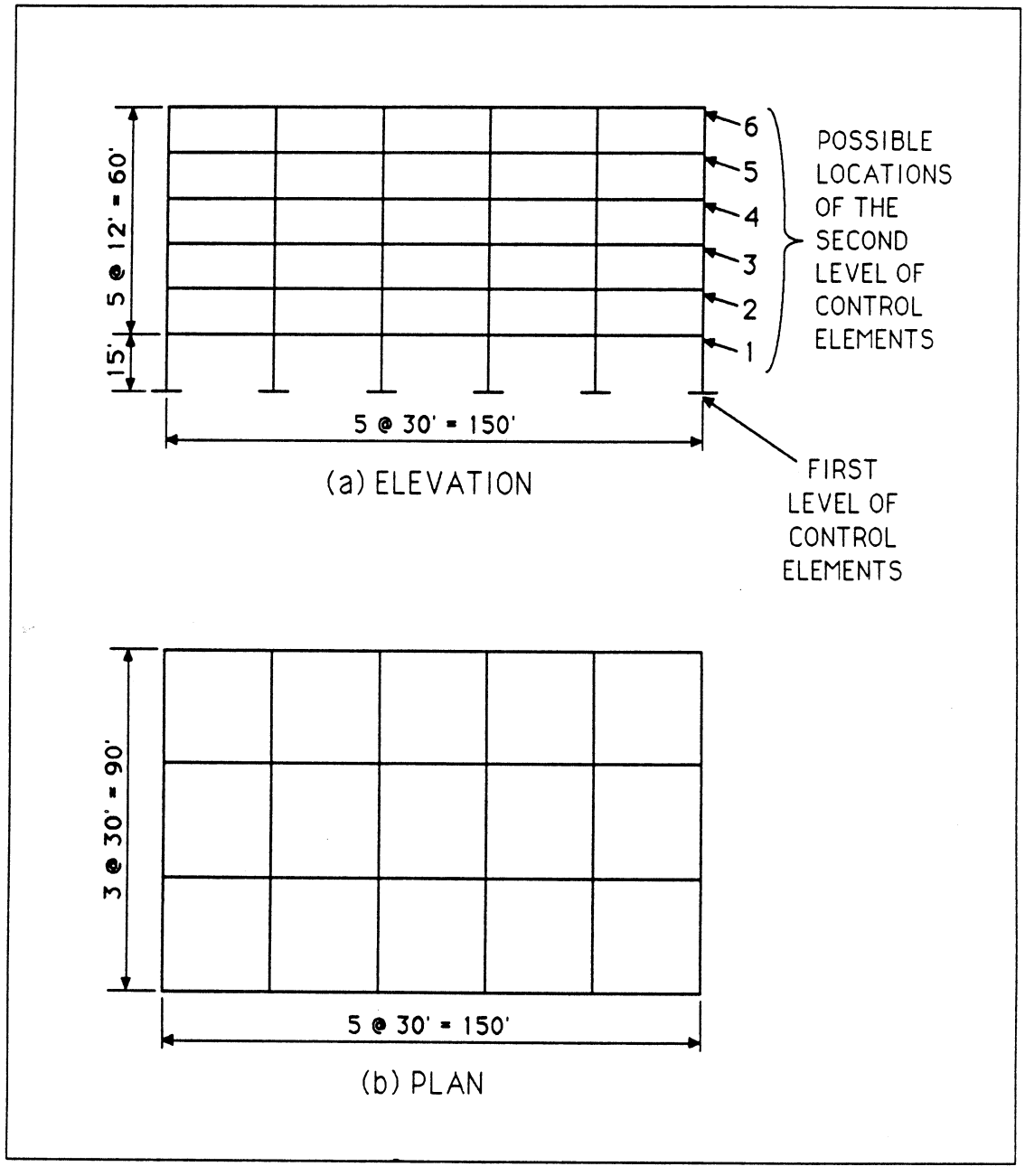

Fig. 1.4 *A six-story building example: a. Elevation; b. Plan*

Table 1.1

Dead loads for the example building

components contributing to dead load	*floors (psf)*	*roof (psf)*
steel plus fire proofing	25	15
steel decking	5	5
light weight concrete slab	30	30
plumbing, ducts, etc.	10	10
partitions	20	0
roofing material	0	10
parapet	0	5
fixed mechanical equipment	0	15
dead load (sum of above)	90	90

Table 1.2

Weight distribution for the 2dof equivalent models

model number	*location of the second level of control elements*(1)	$W_1^{(2)}$ *(kips)*	$W_2^{(3)}$ *(kips)*	W_2/W_1 *ratio*
1	1	50	300	6/1
2	2	100	250	5/2
3	3	150	200	4/3
4	4	200	150	3/4
5	5	250	100	2/5
6	6	300	50	1/6
7(4)	–	350	0	0

(1) *See Fig. 1.4a.*

(2) W_1 = *Weight below the second level of control elements.*

(3) W_2 = *Weight above the second level of control elements.*

(4) *This model corresponds to the base isolated version.*

1.4 Laminated Rubber Bearings

The discussion in this section is intended to provide a broad picture of the behavior of laminated rubber bearings under the combined action of lateral and vertical loads. It is by no means an exhaustive treatment of the subject. As such, it will serve to identify, in approximate ways, the influence of various geometrical parameters affecting the lateral flexibility, the vertical rigidity, and the stability of these commonly used devices. This identification will assist in imposing practical design limits in the formulation of the optimal design which appears in the following chapter.

Natural and synthetic rubbers are viscoelastic materials with low shear moduli (in the neighborhood of 150 *psi*). At the same time these materials are nearly incompressible. In a laminated rubber bearing both these properties are utilized to produce a stub column which is laterally flexible and vertically stiff. As shown in Fig. 1.5, a laminated rubber bearing consists of a column of thin rubber sheets and steel plates strongly bonded together. The role of rubber is to provide low lateral stiffness through shearing deformation, while the steel layers constrain the bulging of rubber under compressive loads and thus help to increase the vertical and tilting stiffness of the bearing.

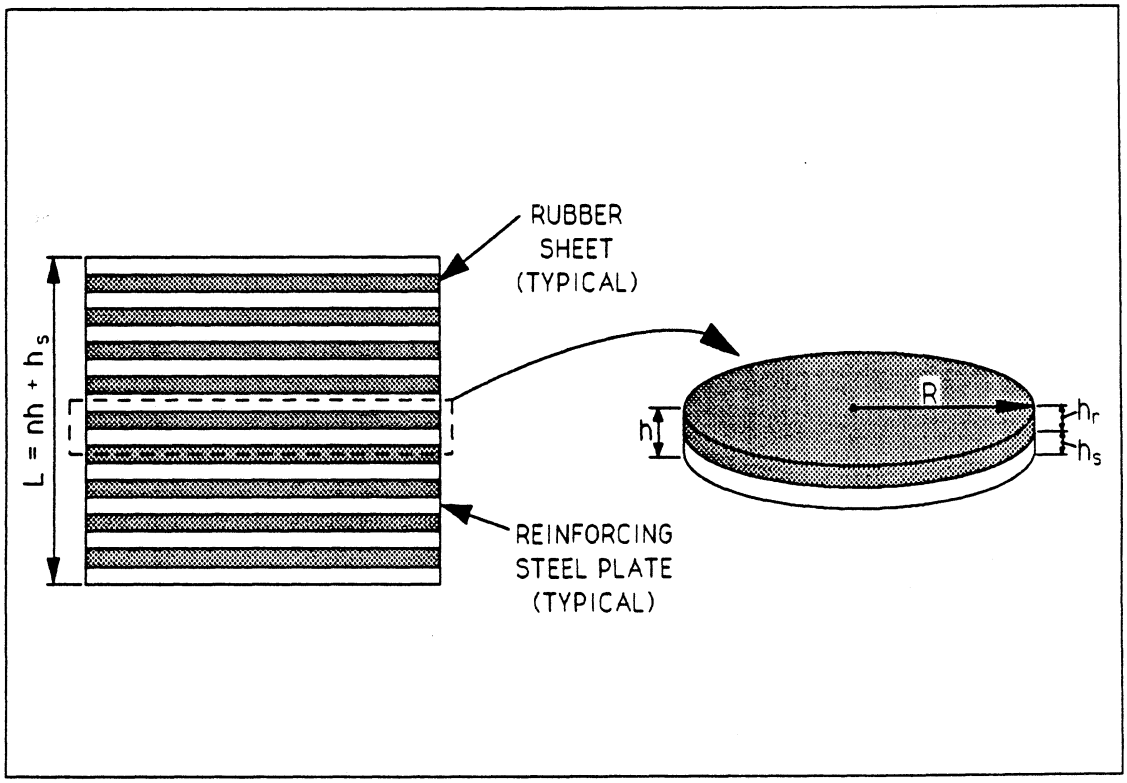

Fig. 1.5 *A circular laminated rubber bearing*

The structural behavior of a rubber layer bonded between parallel stiff plates has been the subject of many analytical, numerical, and experimental investigations (Gent and Meinecke, 1970; Roeder, Stanton, and Taylor, 1987; Herrmann, Ramaswamy, and Hamidi, 1989; Chalhoub and Kelly, 1990). In particular, Chalhoub and Kelly have derived exact solutions for the tilting and compressive stiffness of a circular rubber layer constrained between rigid plates in which they have regarded the rubber as a compressible material. They have verified their findings by experiment and concluded that the incompressibility assumption somewhat overestimates the compressive and tilting stiffness of the rubber layer; especially in cases where the ratio of the diameter of rubber layer to its thickness is large (of the order of 50). For the purpose of this discussion, in which the interest is in an overall description of the effect of geometry on the stiffness and stability of rubber bearings, the simpler results due to incompressibility assumption will be given. For a circular rubber layer of radius R, thickness h_r, and shear modulus G, the vertical, tilting, and lateral stiffnesses are respectively given by

$$\bar{K}_v = \frac{3\pi G R^4}{2h_r^3} \tag{1.1}$$

$$\bar{K}_t = \frac{\pi G R^6}{8h_r^3} \tag{1.2}$$

$$\bar{K}_l = \frac{\pi G R^2}{h_r} \tag{1.3}$$

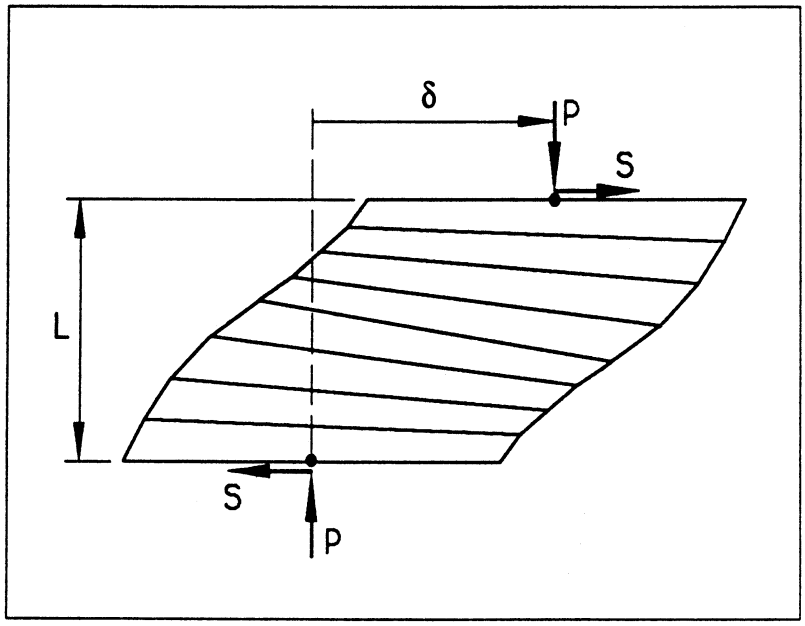

Fig. 1.6 *Lateral deformation of a laminated rubber bearing*

In building applications, the lateral stiffness of a laminated rubber bearing is reduced due to the presence of axial load. Consider the usual case of a bearing restrained against rotation at both ends and subjected to a combined action of a shear force S and a compressive force P. As shown in Fig. 1.6, the resulting lateral deformation is a combination of tilting and shearing of the individual rubber layers. Let the bearing be composed of a stack of n individual rubber units of the same geometry. As shown in Fig. 1.5, each unit consists of a rubber layer of thickness h_r and a steel layer of thickness h_s. The total thickness of the unit, h, is therefore $h_r + h_s$ and the total length of the bearing, L, is $nh + h_s$. Under these circumstances, the lateral displacement of one end of the bearing with respect to the other end, δ, can be written in the following form (Haringx, 1948; Gent, 1964)

$$\delta = \frac{SL}{P}\left[\left(1 + \frac{nP}{L\bar{K}_l}\right)\frac{tan\frac{1}{2}qL}{\frac{1}{2}qL} - 1\right] \tag{1.4}$$

in which the quantity q is computed from

$$q^2 = \frac{nP}{L\bar{K}_t}\left(1 + \frac{nP}{L\bar{K}_l}\right) \tag{1.5}$$

The lateral stiffness of a laminated rubber bearing K_l can be directly evaluated from the load-deflection relationship given by (1.4):

$$K_l = \frac{S}{\delta} = \frac{\bar{K}_l}{n}\left[\frac{\frac{nP}{L\bar{K}_l}}{\left(1 + \frac{nP}{L\bar{K}_l}\right)\frac{tan\frac{1}{2}qL}{\frac{1}{2}qL} - 1}\right] \tag{1.6}$$

In this expression, as either $P \to 0$ or $\bar{K}_t \to \infty$, $K_l \to \frac{\bar{K}_l}{n}$, which is the result that would be obtained if the displacement consisted entirely of a simple shear of all n units in the bearing. This can be verified in conjunction with (1.5) by noting that, in both instances as $P \to 0$ or as $\bar{K}_t \to \infty$, $q \to 0$ and thus in the limit

$$\frac{tan\frac{1}{2}qL}{\frac{1}{2}qL} = 1$$

which together with (1.6) implies that $K_l = \frac{\bar{K}_l}{n}$.

Under the combined action of S and P and for the particular boundary conditions considered (*i.e.* no rotation of the ends), (1.4) is a statement of the bearing's equilibrium from which the critical buckling load, P_c, can be derived. Note that as $\frac{1}{2}qL \to \frac{\pi}{2}$, $\delta \to \infty$, so that P_c corresponds to $q = \frac{\pi}{L}$. With P_c and $\frac{\pi}{L}$ in place of P and q, respectively, (1.5) becomes

$$\frac{\pi^2}{L^2} = \frac{nP_c}{L\bar{K}_t}\left(1 + \frac{nP_c}{L\bar{K}_l}\right)$$

from which

$$P_c = \frac{L\bar{K}_l}{2n}\left[\left(1+\frac{4\pi^2\bar{K}_t}{L^2\bar{K}_l}\right)^{\frac{1}{2}}-1\right] \tag{1.7}$$

For large shearing stiffness $\bar{K}_l$ and large column length L such that

$$\frac{4\pi^2\bar{K}_t}{L^2\bar{K}_l} \ll 1$$

the expression in the brackets in (1.7) can be approximated as

$$\frac{2\pi^2\bar{K}_t}{L^2\bar{K}_l}$$

which, using (1.7) and taking $L = nh$ (for $h_s \ll nh$), leads to the expression for the Euler buckling load:

$$P_c = \frac{\pi^2\bar{K}_t}{nL} = \frac{\pi^2\bar{K}_t}{nL}\frac{h}{h} = \frac{\pi^2\bar{K}_t h}{L^2} = \frac{\pi^2 EI}{L^2} \tag{1.8}$$

in which E[1] is the modulus of elasticity and I is the moment of inertia of the column.

Regarding the buckling load of rubber bearings, the conditions are quite different in that the shearing stiffness $\bar{K}_l$ and the column length L are both small while the tilting stiffness $\bar{K}_t$, due to the restraining effect of the steel layers, is large compared to $\bar{K}_l$. Under these conditions the expression inside the brackets in (1.7) can be approximated as

$$\frac{2\pi}{L}\left(\frac{\bar{K}_t}{\bar{K}_l}\right)^{\frac{1}{2}}$$

which, using (1.7), results in

$$P_c = \frac{\pi}{n}\left(\bar{K}_t\bar{K}_l\right)^{\frac{1}{2}} \tag{1.9}$$

Substituting $\bar{K}_t$ and $\bar{K}_l$ from (1.2) and (1.3) into (1.9), the buckling load takes the following form

$$P_c = \frac{\sqrt{2}\pi^2 GR^4}{4nh_r^2} \tag{1.10}$$

The vertical stiffness of a rubber bearing K_v is obtained by connecting n springs of constant $\bar{K}_v$ in series. This leads to $K_v = \frac{\bar{K}_v}{n}$ which using (1.1) takes the form

$$K_v = \frac{3\pi GR^4}{2nh_r^3} \tag{1.11}$$

[1] $E = 3G$ for incompressible materials

In practice the vertical stiffness K_v is at least 500 times greater than the lateral stiffness K_l as given by (1.6). This requirement together with an examination of (1.2) and (1.3) indicate that the ratio $\frac{\bar{K}_t}{K_l}$ assumes a large value[2] of the order of 5000. Furthermore, in building applications the laminated rubber bearing is designed such that there is a safety factor of at least 2 against buckling (Derham and Thomas, 1983). Recalling that through the assumption of incompressibility of the rubber material the buckling load as given by (1.10) is somewhat overestimated, an even higher safety factor can be justified. Under these circumstances, the lateral stiffness K_l as given by (1.6) will not be significantly lower than its limiting value as $\bar{K}_t \to \infty$. It then follows that, as a first approximation $K_l = \frac{\bar{K}_l}{n}$ which upon using (1.3) becomes

$$K_l = \frac{\pi G R^2}{n h_r} \tag{1.12}$$

For the purpose of design, in addition to imposing lower limits on the buckling load and the vertical stiffness of a rubber bearing, the strains must also be limited to allowable values. Consistent with the formulation of the presented theory, it is assumed than the steel layers are sufficiently thick and thus incur low strains. Moreover, the vertical stiffness of the bearing is assumed large enough so as to keep the axial strain in the rubber layers within acceptable limits. The shearing strain in the rubber layer, due to the lateral flexibility of the bearing, can however be quite large and must be limited to allowable values. As reported by Roeder and Stanton (1983), the shearing strain, which is measured in terms of the lateral displacement δ divided by the total thickness of the rubber material nh_r, should be limited to 50%. Higher percentages can be justified in certain situations (Kelly and Skinner, 1979).

In the application of the modular scheme the objective is to reduce the maximum level of acceleration which is imparted to the structure as a result of earthquake ground motion. This is accomplished by insertion of flexible control elements which in turn reduce the fundamental frequency of the structure. As the fundamental frequency decreases, so does the level of acceleration. At the same time, however, the displacement demand on the control elements will increase. From the preceding discussion, it can be noted that as the displacement demand on the control elements increases, it will be increasingly more costly to satisfy the requirements for vertical stiffness, stability, and shearing strain. Consequently, in an optimal design formulation, imposing an upper bound on the displacement of the control elements can be viewed as a resource constraint. The remainder of this section serves to illustrate this point.

[2]Note that typically the ratio $\frac{R}{h_r}$ is of the order of 50.

Consider a base isolated structure idealized as a single degree of freedom system. The fundamental frequency, $\bar{\omega}$, of this structure is given by

$$\bar{\omega} = \sqrt{\frac{K_l}{M}} \tag{1.13}$$

in which M is a fraction of the total mass corresponding to one control element. For the expected range of frequencies of this structure, a design displacement response spectrum, d, which signifies the maximum displacement of the control elements, can be approximated as

$$d = \frac{\alpha}{\bar{\omega}} \tag{1.14}$$

in which α is a positive constant.

From (1.13) and (1.14) it is clear that as K_l decreases so does $\bar{\omega}$ and thus the displacement will increase. Let the total shearing strain be limited to a prescribed value β. Since the shearing strain is defined as the ratio $\frac{d}{nh_r}$, the most economical choice for nh_r will be

$$nh_r = \frac{d}{\beta} \tag{1.15}$$

Recall that nh_r is the total rubber thickness used in the construction of the control element. Using (1.13) to (1.15), the lateral stiffness can be written as

$$K_l = \frac{M\alpha^2}{\beta^2(nh_r)^2} \tag{1.16}$$

Equating this expression for K_l to that given by (1.12), leads to

$$R^2 nh_r = \frac{M\alpha^2}{\pi\beta^2 G} = constant \tag{1.17}$$

For convenience, using (1.12), one can rewrite (1.10) and (1.11) respectively in the following forms

$$P_c = \frac{\sqrt{2}\pi R^2}{4h_r} K_l \tag{1.18}$$

$$K_v = \frac{3R^2}{2h_r^2} K_l \tag{1.19}$$

With the aid of the sequence of equations (1.14) to (1.19), it is now possible, more directly, to examine the effect of a decrease in the fundamental frequency $\bar{\omega}$ on the design of a control element. Denoting by $\downarrow$ and $\uparrow$, respectively, a decrease and an increase in the adjacent quantity, it can be noted that:

1. From (1.14), as $\bar{\omega} \downarrow$, $d \uparrow$.

2. From (1.15), as $d \uparrow$, $(nh_r) \uparrow$.

3. From (1.16), as $(nh_r) \uparrow$, $K_l \downarrow$.

4. From (1.17), as $(nh_r) \uparrow$, $R \downarrow$.

5. From (1.18) and for fixed h_r, as $R \downarrow$ and $K_l \downarrow$, $P_c \downarrow$.

6. From (1.19) and for fixed h_r, as $R \downarrow$ and $K_l \downarrow$, $K_v \downarrow$.

In order to keep P_c and K_v above prescribed minimum values, one possible choice is to use smaller h_r which will also result in an increase in the number of rubber layers n and thus the cost of construction. Another choice is to restart the design cycle with larger R and nh_r which again increases cost. Therefore the smaller K_l, or the larger d is, the more costly will be the construction of the control element. The foregoing argument is generally applicable to other possible types of control elements described by Lin, Tadjbakhsh, Papageorgiou, Ahmadi (1990), Mokha, and Constantinou (1990). Without the inclusion of any particular control element design in the optimization of modular structures, it is therefore concluded that a cap on the extent of the intermodule lateral displacements can be viewed as one constraint on the available resources.

1.5 The Optimization Problem

In a modular structure a wide range of stiffness and damping coefficients can be assigned to the control elements without significantly affecting the basic design for gravity and interstory drift limits. This property facilitates a manageable optimization formulation for the elastic response to earthquakes. Furthermore, by virtue of its form, the modular structure can be physically constructed as to reflect the solution to its mathematical optimization problem.

With a given earthquake excitation and for known constraints, the problem is to search for the values of control element stiffness and damping coefficients which correspond to the minimum of a prescribed objective function. The objective function represents a measure of one or several of the structural response parameters related to various parts of the structure. The constraint functions establish limits on those response parameters that do not explicitly appear in the objective function. Depending on the nature of the problem and the stage of analysis, the objective and any of the constraint functions can be interchanged.

The most meaningful objective function is the one that signifies the portion of the total cost of the building ascribed to earthquake protection. Arriving at a mathematical expression for this cost function, even for a fixed structural layout, is not a simple task. One is, therefore, forced to simplify the matter by searching for an objective function which represents the *best measure* of an explicit cost function. At an early stage of analysis the total base shear represents an acceptable measure of cost. Subsequently, the ratio of the total overturning moment to the total base shear, or the sum of shear forces and overturning moments in each module, can be considered as more refined measures of cost. Some level of engineering judgment is necessary for further refinement of the objective function. Several seemingly appropriate objective functions that are indistinguishable by engineering judgment alone can always be tested for preference.

With respect to the modular structures, one objective is to reduce the maximum accelerations imparted to each module. An equally important objective is to reduce the cost of the control elements by reducing the demand on their lateral displacement. As pointed out for the case of rubber bearings in Section 1.4, the smaller the lateral displacement demand the smaller the total height of the rubber material and hence the fewer the number of steel reinforcements, all of which translate into savings in construction cost. It was also pointed out that the control elements placed at higher locations will incur smaller gravity loads and thus contribute to savings.

As described in Section 1.3, the two degree of freedom models of a six-story building will be used in Chapter 3 for the optimal design illustrations. For performance evaluation of the various possible modular mass ratios of this structure, a consistent objective function is the base shear, and a consistent set of constraints, without involving the details of the particular control elements used, is an upper limit on the lateral displacement of the control elements at all levels. A precise mathematical formulation of the optimization problem will be given in Section 3.4.

1.6 Analytical Methods

Various methods of evaluation of structural elastic response to earthquake excitation are reviewed in this section. In this regard, only the maximum values of response quantities are of interest. These methods fall in the broad categories of the response spectrum approach, the time history analysis, and the random vibration technique. In this same sequence, each method is discussed in an attempt to point out their advantages and shortcomings relevant to the process of optimal design.

The simplest method is the standard modal superposition. This requires imposing some proportionality restriction on the damping matrix so that the eigenvectors of the undamped eigenvalue problem produce a set of uncoupled modal equations. Then, the available earthquake response spectra are used to find the maximum value of modal response parameters. The maximum modal responses thus obtained are finally combined by the complete quadratic combination or the square root of sum of the squares methods to arrive at an estimate of the total response (Wilson, Der Kiureghian, and Bayo, 1981; Berg, 1989). The most serious problem with this approach is the proportional damping restriction. The damping matrix, due to the pattern in which the control elements are *installed*, is tridiagonal. This also results in a tridiagonal stiffness matrix. For the damping matrix to be proportional, and at the same time *installable*; that is, to conform to the installation pattern of the control elements, it must be proportional to the stiffness matrix. This type of proportionality confines the variables of the optimization problem to the stiffness coefficients. Furthermore, this form of damping produces increasingly more damping in the higher modes. This is not economically desirable since only the lowest modes have dominant contributions to the total response.

In structures with supplemental damping devices of known characteristics, one successful method of analysis is to start with the known damping matrix, use the undamped modes to dispose of mass- and stiffness-coupling, and then to integrate numerically only the first few significant damping-coupled modal equations (Clough and Mojtahedi, 1976). This method produces accurate results while avoiding considerable computational effort for large systems. For the modular structure, the number of equations will not exceed the number of modules, therefore, the exact numerical integration of equilibrium equations does not pose a serious drawback. The formulation of optimization problems in which time dependent quantities, in particular the maximum values of these quantities in a given time interval, are involved, can also be managed by well established methods (Haftka and Kamat, 1985; Haug and Arora, 1979). The difficulty is however with the character of earthquake excitation and the resulting structural response. To illustrate, consider a simple damped oscillator subjected to a real earthquake acceleration record at the base. Let the mass and the damping coefficient have fixed values. Consider finding the value of the spring constant for which the acceleration of the mass is minimized while its maximum displacement relative to base is restricted to a certain limit. This is a simple idealization of an optimal design formulation for a low rise base isolated structure. The solution can be found by constructing the acceleration and displacement response

spectra associated with the given base acceleration record. As shown in Fig. 1.7, although both spectra will have jagged patterns, the acceleration spectrum tends to decrease and the displacement spectrum tends to increase with decreasing values of the spring constant. Having a barrier level for the displacement, the optimum design can be identified as that value of the spring constant, k^*, for which the displacement response spectrum crosses the barrier.

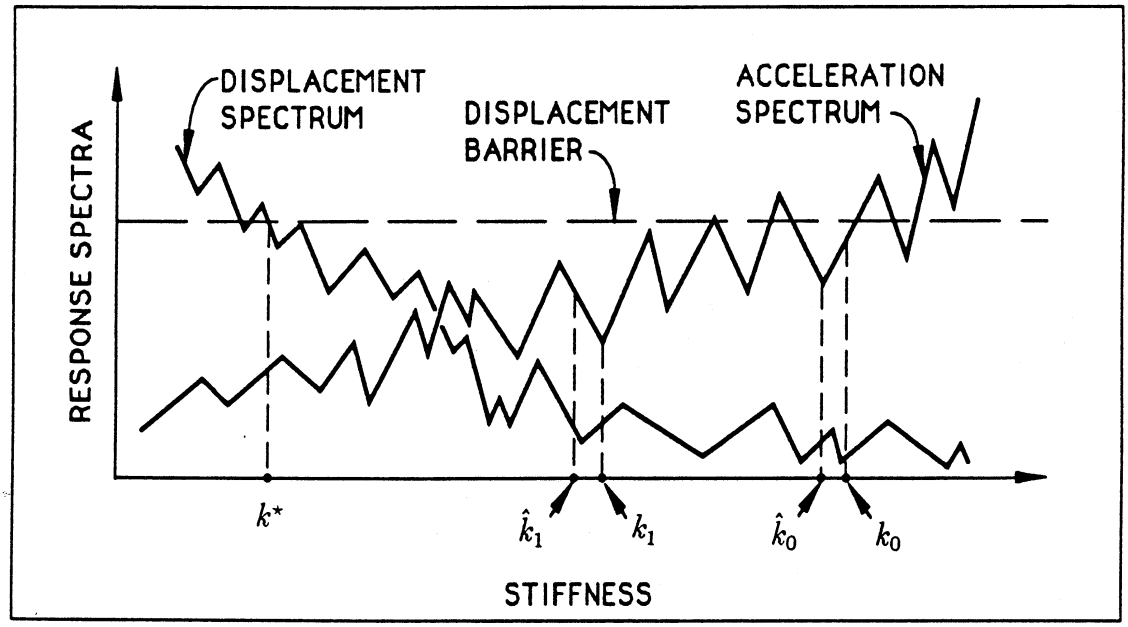

Fig. 1.7 *Jaggedness of earthquake response spectra*

In a mathematical search technique, at every advancement to a new value for the spring constant, a certain reduction in acceleration is sought without violating the displacement barrier. With reference to Fig. 1.7, starting at the initial point k_0, the search will quickly halt at $\hat{k}_0$ — a local minimum within the boundary of the feasible domain. Restarting the process at another point, such as k_1, will again quickly produce another local minimum at $\hat{k}_1$ close to the initial point. Because of the jagged nature of the response spectra, there are numerous local minima which could be far away from the actual optimum design k^*. Consequently the time domain approach with actual earthquake records is not an effective way of tackling the optimal design problems.

It is possible to generate artificial earthquake acceleration records which are compatible with a given smooth design response spectrum (Gasparini and Vanmarcke, 1976; Scanlan and Sachs, 1974). This requires generating first an excitation power spectral density *(psd)* function that produces the given smooth response spectrum, and next finding an artificial acceleration time history compatible with the computed

psd function. The end results are a time series and a frequency decomposition which both produce the parent smooth design response spectrum. The time series can be used in the time domain formulation of the optimization problem, and the *psd* function can be used in the corresponding frequency domain formulation. In both instances the damping coefficients can be considered as variables of the optimization problem without any proportionality restrictions.

For the present research, the frequency domain formulation is adopted since it requires less computation time. The framework of this formulation, using the probabilistic methods of random vibration, is presented in Chapter 2. Within this framework, a method of relating smooth design response spectra to the *psd* of excitation is devised. The spectrum-compatible excitation *psd* thus obtained will be used in Chapter 3 in the investigation of the optimal design of modular structures.

CHAPTER 2

STRUCTURAL RESPONSE TO EARTHQUAKES

2.1 Introduction

The behavior of a building subjected to an earthquake is assessed based on the extreme value of the response quantities of interest. When the building can be modeled as a single degree of freedom system, a design response spectrum furnishes the extreme value of response with a certain probability of exceedance. For a multiple degree of freedom system, the response spectrum approach can be extended to assess the extreme value of response only under the restriction of proportionality of damping (Wilson, Der Kiureghian, and Bayos, 1981; Der Kiureghian, 1980a). In conventional structures with low damping, the assumption of damping proportionality provides computational convenience and produces acceptable results. In structures in which damping devices are intentionally added to improve their behavior in an optimal sense, the proportionality assumption may no longer apply. In such cases the probabilistic methods of random vibration provide a rational basis for evaluation of response to earthquakes.

In the application of random vibration methodology the earthquake excitation is characterized by its power spectral density *(psd)* function. Under certain conditions the *psd* of any quantity of response can be written in terms of the *psd* of excitation. The knowledge of the *psd* of a response quantity leads to a set of statistical averages from which the extreme value of response can be estimated. This holds true for a system with any number of degrees of freedom. For a single degree of freedom system, the extreme values are available from a design response spectrum. This suggests that the *psd* of excitation and a design response spectrum derived from the same excitation are related.

The most widely used *psd* for strong motion earthquakes is that due to Kanai (1957) and Tajimi (1960). It is a three-parameter *psd* which represents a white noise excitation of constant *psd*, S_0, filtered through a single degree of freedom spring-

mass-damper model characterized by its frequency, ω_g, and damping ratio, ξ_g. The parameters of this model (S_0, ω_g, ξ_g) were extensively studied by Lai (1982) who based his investigation on 140 actual strong motion acceleration records. His statistical study, however, does not subcategorize these records with regard to specific site conditions, earthquake magnitude, maximum ground acceleration, and other pertinent factors which are of interest for design purposes. Lin, Tadjbakhsh, Papageorgiou, and Ahmadi (1990), in their evaluation of the performance of earthquake isolation systems, proposed a seven-parameter filtered white noise whose parameters are derived from seismological earthquake source spectra. They used two different spectral source models independently, but the scope of their study does not extend to resolving the discrepancies between the two models.

Design response spectra, on the other hand, are more widely available and used by the engineering profession. In particular, the design response spectra provided by Mohraz (1976), Seed, Ugas, and Lysmer (1976) are site-specific and form the basis of spectra recommended for design by the Building Seismic Safety Council (BSSC, 1988). Because the application of random vibration techniques requires a knowledge of the *psd* of excitation, it is desirable to establish methods of deriving *psd* functions from design response spectra using the available probabilistic framework. Pfaffinger (1983) has established one such method based on an extreme value probability distribution derived from a Poisson model of barrier crossings. It has been shown by Der Kiureghian (1980b) that this model tends to overestimate the mean extreme value of the random process. In this chapter the more accurate extreme value probability distribution of Vanmarcke (1975) is employed and the method presented is computationally simpler than that suggested by Pfaffinger. It leads to a functional form directly relating the mean response spectrum to the *psd* of excitation.

2.2 Excitation and Response Relations

The earthquake that may strike the base of a building during its expected lifetime is considered to be a sample of a stationary normal process with zero mean. Since the building is modeled as a linear time invariant system, the response will also be stationary normal with zero mean (Nigam, 1983). The excitation is the base acceleration, $\ddot{x}_b$, and the response is any quantity of interest, z. Both the excitation and the response are characterized by their one-sided *psd* which are functions of the circular frequency, ω. Under the stationarity assumption, the excitation *psd*, $S_{\ddot{x}_b}$, is

related to the response *psd*, S_z, by the following equation (Nigam, 1983)

$$S_z = |H_z|^2 S_{\ddot{x}_b} = Q_z S_{\ddot{x}_b} \tag{2.1}$$

in which H_z is the complex frequency response associated with the response quantity z; and $Q_z = |H_z|^2$ is the corresponding transfer function. The complex frequency response can be found by substituting $\ddot{x}_b = exp(i\omega t)$ and $z = H_z \ddot{x}_b$ in the differential equations of motion. Properties of S_z, significant to the subsequent treatment, are the first three spectral moments of the process z, namely λ_0, λ_1, and λ_2, determined from (Nigam, 1983)

$$\lambda_j = \int_0^\infty \omega^j S_z d\omega \ ; \quad j = 0, 1, 2 \tag{2.2}$$

The extreme values of the response process z in a fixed interval of time τ constitute the sample space of a random variable denoted here as z^e. Knowledge of the probability distribution of z^e enables one to estimate statistical averages of the extreme values, in particular, the mean and the standard deviation of z^e which are of principal interest in evaluation of response to earthquakes. A comprehensive treatment of the probability concepts relating to the random variable z^e is given by Nigam (1983). Here, for the sake of brevity, only important results which support the development in the next section are presented.

The probability distribution of z^e is closely related to the probability distribution of the first passage time t_f at which the parent process z crosses a symmetric barrier level $\pm z_0$. This is true since, for the same barrier level, the probability that t_f is greater than τ is the same as the probability that z^e does not cross the barrier in the time interval τ. Vanmarcke (1975) has derived an expression for the probability distribution of the first passage time of a stationary normal process with zero mean in which he has taken into account the statistical dependence between barrier crossings of the process. Using Vanmarcke's expression, the probability distribution function, $P(z_0)$, signifying the probability that z^e is less than z_0, is given by

$$P(z_0) = \left[1 - exp\left(\frac{-r^2}{2}\right)\right] exp\left[-2\nu\tau \frac{1 - exp\left(-\sqrt{\frac{\pi}{2}} q^{1+b} r\right)}{exp\left(\frac{r^2}{2}\right) - 1}\right] \tag{2.3}$$

in which $r = z_0/\sqrt{\lambda_0}$ is the normalized barrier level; and the spectral parameters ν and q are determined from

$$\nu = \frac{1}{2\pi}\sqrt{\frac{\lambda_2}{\lambda_0}} \tag{2.4}$$

$$q = \sqrt{1 - \frac{\lambda_1^2}{\lambda_0 \lambda_2}} \tag{2.5}$$

The parameter b is an empirical constant with the value 0.2. The spectral parameter ν is a measure of the central frequency of the random process, while q is a measure of the dispersion of the *psd* function about the central frequency.

Based on the probability distribution (2.3), Der Kiureghian (1980b) has derived semi-empirical expressions for the mean and the standard deviation of z^e. The mean or expected value, $E[z^e]$, is given by

$$E[z^e] = \left(\sqrt{2ln\nu_0\tau} + \frac{0.5772}{\sqrt{2ln\nu_0\tau}}\right)\sqrt{\lambda_0} \tag{2.6}$$

and the standard deviation, σ_{z^e}, is evaluated from

$$\sigma_{z^e} = \begin{cases} \left[\frac{1.2}{\sqrt{2ln\nu_0\tau}} - \frac{5.4}{13+(2ln\nu_0\tau)^{3.2}}\right]\sqrt{\lambda_0} \; ; & \nu_0\tau > 2.1 \\ 0.65\sqrt{\lambda_0} \; ; & \nu_0\tau \leq 2.1 \end{cases} \tag{2.7}$$

In the expressions for $E[z^e]$ and σ_{z^e}, the spectral parameter ν_0 is expressed as

$$\nu_0 = \begin{cases} 2\left(1.63q^{0.45} - 0.38\right)\nu \; ; & q < 0.69 \\ 2\nu \; ; & q \geq 0.69 \end{cases} \tag{2.8}$$

It is convenient to rewrite (2.6) in the following form

$$E[z^e] = p\sqrt{\lambda_0} \tag{2.9}$$

where

$$p = \sqrt{2ln\nu_0\tau} + \frac{0.5772}{\sqrt{2ln\nu_0\tau}} \tag{2.10}$$

In summary, for any response quantity z of a multiple degree of freedom system, the corresponding transfer function Q_z can be determined from the differential equations of motion. Having the *psd* of base acceleration $S_{\ddot{x}_b}$, the *psd* of response S_z is given by (2.1). Using (2.2), the spectral moments of the response process can then be evaluated. Finally, the mean extreme value of response becomes known using (2.6) and (2.8). This procedure is repeated for as many number of response quantities as necessary. In particular, for a single degree of freedom system characterized by its natural frequency and damping ratio, the procedure furnishes the mean extreme value of any response quantity of interest. If, for instance, the mean extreme value of the absolute acceleration of the mass is sought, the outcome determines the ordinate of one point on a mean acceleration response spectrum. This is of significance since, as will be shown in the next section, given an acceleration response spectrum, one can proceed backwards through the above procedure and arrive at the *psd* of base acceleration. The *psd* of base acceleration is a characterization of the base motion only and can be applied to any system with single or multiple degree of freedom.

2.3 Power Spectral Density and Response Spectrum Relation

A linear, viscously damped, single degree of freedom system subjected to base excitation is described by

$$\ddot{x} + 2\xi\bar{\omega}\dot{x} + \bar{\omega}^2 x = 2\xi\bar{\omega}\dot{x}_b + \bar{\omega}^2 x_b \tag{2.11}$$

where $\ddot{x}$, $\dot{x}$, and x are, respectively, the absolute acceleration, absolute velocity, and absolute displacement of the mass; $\dot{x}_b$ and x_b are, respectively, the velocity and displacement of the base; ξ is the system damping ratio; and $\bar{\omega}$ is the system natural frequency. It is assumed that the excitation process is the base acceleration, $\ddot{x}_b$, and the response process is the absolute acceleration of the mass, $\ddot{x}$. The complex frequency response, $H_{\ddot{x}}$, associated with $\ddot{x}$, is obtained by substituting $\ddot{x}_b = exp(i\omega t)$ and $\ddot{x} = H_{\ddot{x}}\ddot{x}_b$ in (2.11) :

$$H_{\ddot{x}} = \frac{\bar{\omega}^2 + 2i\xi\bar{\omega}\omega}{\bar{\omega}^2 - \omega^2 + 2i\xi\bar{\omega}\omega} \tag{2.12}$$

in which $i = \sqrt{-1}$.

In what follows, one point of a mean acceleration response spectrum corresponding to specified $\bar{\omega}$ and ξ is considered equivalent to $E[\ddot{x}^e]$ which signifies the mean extreme value of the response process $\ddot{x}$ in the time interval τ. An acceleration response spectrum normalized to a ground acceleration of 1 g, where g is the gravitational acceleration, can be constructed using the log-normal statistical data given by Mohraz (1976). The mean values of his data pertaining to rock deposits are selected for the present study. Mohraz and Elghadamsi (1989) have presented a comprehensive review of the attenuation of maximum ground acceleration for different magnitude earthquakes pertaining to different site conditions. They have noted that the influence of soil condition can generally be neglected when using acceleration attenuation laws. From their data, for a magnitude 7.5 earthquake at a selected distance 10 km from the source of energy release, the mean maximum ground acceleration is estimated to equal 0.5 g. A mean acceleration response spectrum $E[\ddot{x}^e]$ can then be obtained by multiplying the normalized acceleration response spectrum by the mean maximum ground acceleration. Plots of $E[\ddot{x}^e]$ for several values of the damping ratio ξ are shown in Fig. 2.1. The equation form of the plot with 5% damping is

$$E[\ddot{x}^e] = \begin{cases} \frac{\bar{\omega}}{18} g \ ; & 0 \le \bar{\omega} < \omega_0 \\ 1.16g \ ; & \omega_0 \le \bar{\omega} < 50 \\ \left(\frac{33}{\bar{\omega}} + 0.5\right) g \ ; & \bar{\omega} \ge 50 \end{cases} \tag{2.13}$$

in which ω_0, in this case, is equal to 20.88 rad/sec. This equation will be used to derive a compatible excitation *psd* function.

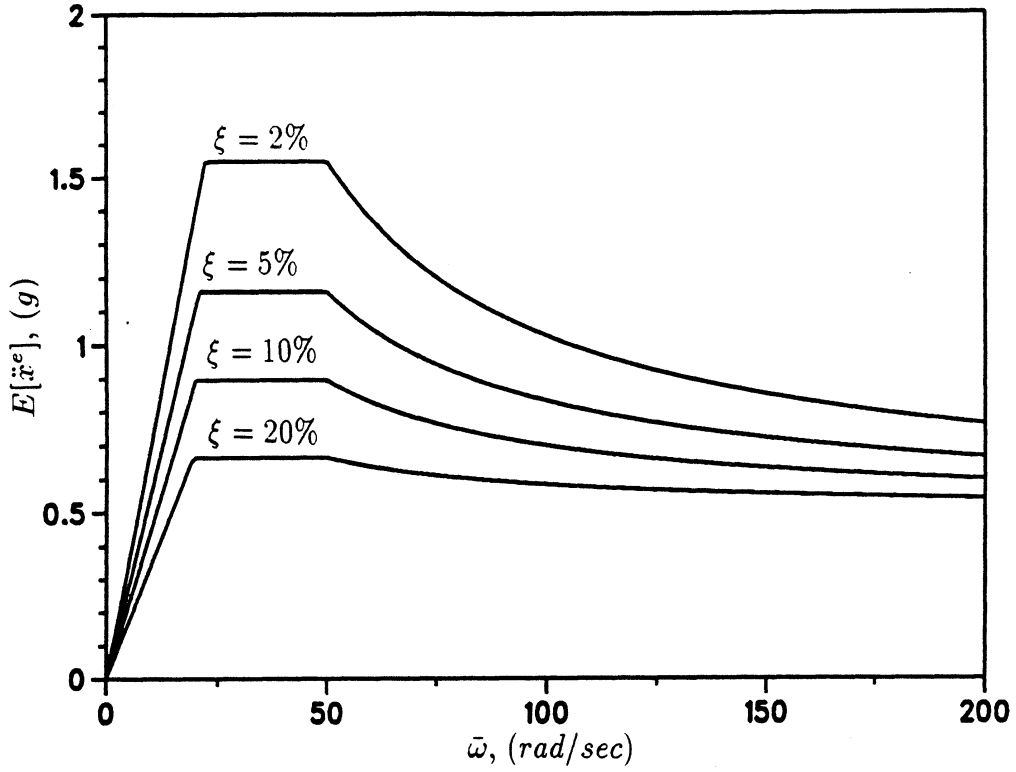

Fig. 2.1 *Mean acceleration response spectra for structures founded on rock deposits*

As is evident from the development in the previous section, the evaluation of a mean acceleration response spectrum $E[\ddot{x}^e]$ compatible with a known excitation *psd* is straightforward. Here, the interest is to do the opposite, that is, to derive the excitation *psd* from a given mean acceleration response spectrum. To begin, it is noted that when ξ and $\bar{\omega}$ are both small, the transfer function associated with (2.12) is a narrow band spike centered at $\bar{\omega}$. Under these conditions, for evaluation of the first spectral moment λ_o, any slowly varying *psd* function $S_{\ddot{x}_b}(\omega)$ can be approximated by a constant *psd* equal to $S_{\ddot{x}_b}(\bar{\omega})$. Consequently, λ_0 can be evaluated analytically using Cauchy's residue theorem (Crandall and Mark, 1963):

$$\lambda_0 = \frac{\pi\bar{\omega}(1+4\xi^2)}{4\xi} S_{\ddot{x}_b}(\bar{\omega}) \tag{2.14}$$

which, neglecting the second power of ξ, leads to

$$S_{\ddot{x}_b}(\bar{\omega}) = \frac{4\xi}{\pi\bar{\omega}}\lambda_0 \tag{2.15}$$

Solving for λ_0 from (2.9) and substituting in (2.15), $S_{\ddot{x}_b}(\bar{\omega})$ takes the form

$$S_{\ddot{x}_b}(\bar{\omega}) = \frac{4\xi}{\pi}\frac{(E[\ddot{x}^e])^2}{\bar{\omega}}\frac{1}{p^2} \tag{2.16}$$

Examination of the sequence of equations (2.10), (2.8), (2.5), (2.4), (2.2), and (2.1) indicates that p^2 is a complicated function of $\bar{\omega}$ whose evaluation requires prior knowledge of $S_{\ddot{x}_b}(\omega)$. It is however a smooth function and can be approximated by a simple function of $\bar{\omega}$ denoted here as ϕ. As suggested by (2.10) and the behavior of the second fraction in (2.16), a simple form for ϕ is a logarithmic function defined as

$$\phi = \begin{cases} b_1 + b_2 ln(\bar{\omega}) \; ; & \bar{\omega} \leq \omega_0 \\ c_1 + c_2 ln(\bar{\omega}) \; ; & \bar{\omega} > \omega_0 \end{cases} \tag{2.17}$$

in which b_1, b_2, c_1, and c_2 are constant coefficients as yet to be determined. With this approximation and interchanging $\bar{\omega}$ for ω, (2.16) becomes

$$S_{\ddot{x}_b}(\omega) = \frac{4\xi}{\pi} \frac{(E[\ddot{x}^e])^2}{\omega} \frac{1}{\phi} \tag{2.18}$$

Under the assumption than ξ and $\bar{\omega}$ are both small, (2.18) provides a first approximation to the actual excitation *psd*. The coefficients of ϕ can be evaluated through the following iterative procedure:

1. As an initial guess all coefficients of ϕ in (2.17) are assumed to equal unity.

2. Having ϕ and with an actual mean acceleration response spectrum $E[\ddot{x}^e]$ such as (2.13), $S_{\ddot{x}_b}$ becomes available through (2.18).

3. With $S_{\ddot{x}_b}$ just obtained and the complex frequency response given by (2.12), the sequence of equations (2.1), (2.2)[1], (2.4), (2.5), (2.8), and (2.10) are used to arrive at the quantity p^2 at selected values of $\bar{\omega}$.

4. The data defining p^2 at discrete values of $\bar{\omega}$ are used to compute new coefficients for an improved ϕ. This is done by least squares approximation.

5. If the newly computed coefficients are not close enough to those at the start of iteration, the improved ϕ is used to start another iteration at step 2.

[1]The computation of spectral moments in (2.2) involves numerical integration. The upper limit of integration, although theoretically infinite, can be set equal to a value at which the transfer function $Q_{\ddot{x}}$ is practically zero. A small multiple of $\bar{\omega}$ such as $5\bar{\omega}$ is adequate for the upper limit. Because ϕ cannot physically take nonpositive values, such as occur in (2.17) for small values of ω, the lower limit is selected at a point somewhat beyond the zero of ϕ at $\omega = exp(-b_1/b_2)$. This remedy does not introduce significant error in spectral moment values since the point $\omega = exp(-b_1/b_2)$ is nearly zero.

This procedure provides acceptable results in a few iterations. To illustrate, $E[\ddot{x}^e]$ of (2.13) which corresponds to $\xi = 0.05$ is used. The fixed interval of time τ in which the statistics of the response process are examined is assumed to equal the duration of the stationary excitation process. Based on numerous strong motion models and duration studies reported by Mohraz and Elghadamsi (1989), it is reasonable to assume that, for a magnitude 7.5 earthquake recorded on rock sites 10 *km* from the source of energy release, the duration of the stationary part of the excitation process is 25 *sec.* For evaluation of discrete values of p^2 in step 3, the system natural frequencies are selected from 2 *rad/sec* to 20.88 *rad/sec* in 10 increments; and from 20.88 *rad/sec* to 200 *rad/sec* likewise in 10 increments. With these preliminary data, the unknown coefficients are computed and listed in Table 2.1 for every iteration. Convergence, based on equality of successive coefficients to four decimal places, is achieved in 6 iterations.

Table 2.1

Iterative convergence of coefficients in (2.17)

	coefficients			
iteration	b_1	b_2	c_1	c_2
0	1.0000	1.0000	1.0000	1.0000
1	5.0040	1.4024	0.9793	2.6559
2	5.3110	1.2773	1.2401	2.6231
3	5.3343	1.2652	1.2464	2.6221
4	5.3364	1.2641	1.2465	2.6221
5	5.3366	1.2640	1.2465	2.6221
6	5.3366	1.2640	1.2465	2.6221

The function ϕ having the coefficients in the last row of Table 2.1, and the corresponding quantity p^2 are plotted in Fig. 2.2. The agreement indicates that ϕ as defined by (2.17) is an appropriate approximation to the quantity p^2 as evaluated from (2.10).

As already mentioned, (2.18) is valid only for small values of $\bar{\omega}$. To find the maximum value of $\bar{\omega}$ for which (2.18) holds, it suffices to compare $E[\ddot{x}^e]$ as computed from (2.9) to $E[\ddot{x}^e]$ as given by (2.13). Using the coefficients in the last row of Table 2.1, $S_{\ddot{x}_b}$ becomes available. The corresponding $E[\ddot{x}^e]$ can therefore be computed from (2.9). The result, denoted as $E[\ddot{x}^e](approx)$, is plotted in Fig. 2.3. In the same figure $E[\ddot{x}^e]$ as given in (2.13) is also plotted and denoted as $E[\ddot{x}^e](target)$.

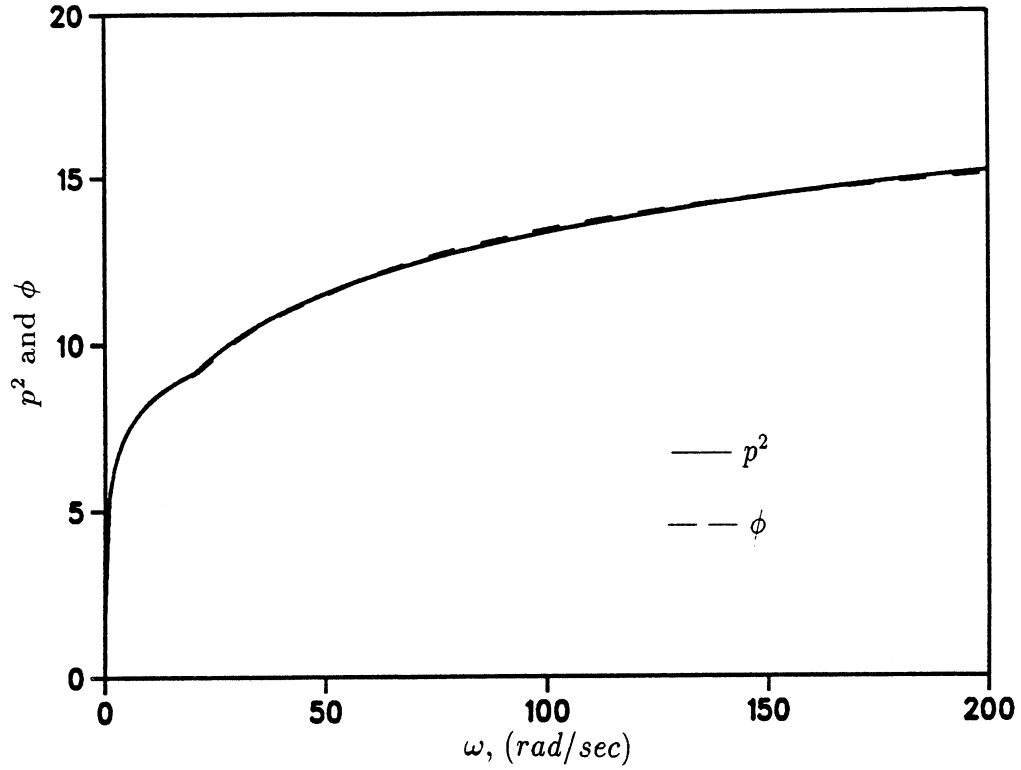

Fig. 2.2 *Agreement between the functions ϕ and p^2*

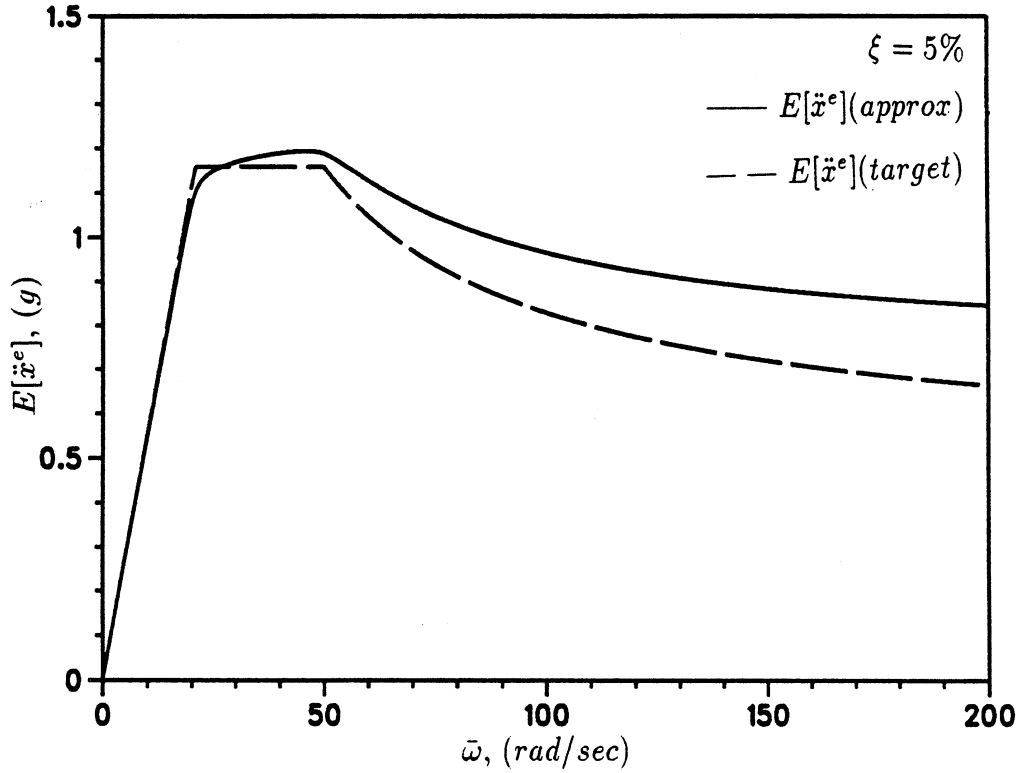

Fig. 2.3 *Matching of the response spectra based on (2.18)*

From Fig. 2.3 it is clear that up to a frequency of about ω_0=20.88 rad/sec the two curves are similar. Beyond this frequency $E[\ddot{x}^e](approx)$ falls above $E[\ddot{x}^e](target)$ and the difference increases slowly with increasing frequency. This discrepancy can be corrected by multiplying the right hand side of (2.18) by a slowly decaying function of ω defined as

$$\psi = \begin{cases} 1 \ ; & \omega \leq \omega_0 \\ exp\left(\frac{\omega_0 - \omega}{\alpha}\right) \ ; & \omega > \omega_0 \end{cases} \tag{2.19}$$

where α is a positive constant to be determined iteratively. With the introduction of the correcting function ψ, (2.18) becomes

$$S_{\ddot{x}_b} = \frac{4\xi}{\pi} \frac{(E[\ddot{x}^e])^2}{\omega} \frac{\psi}{\phi} \tag{2.20}$$

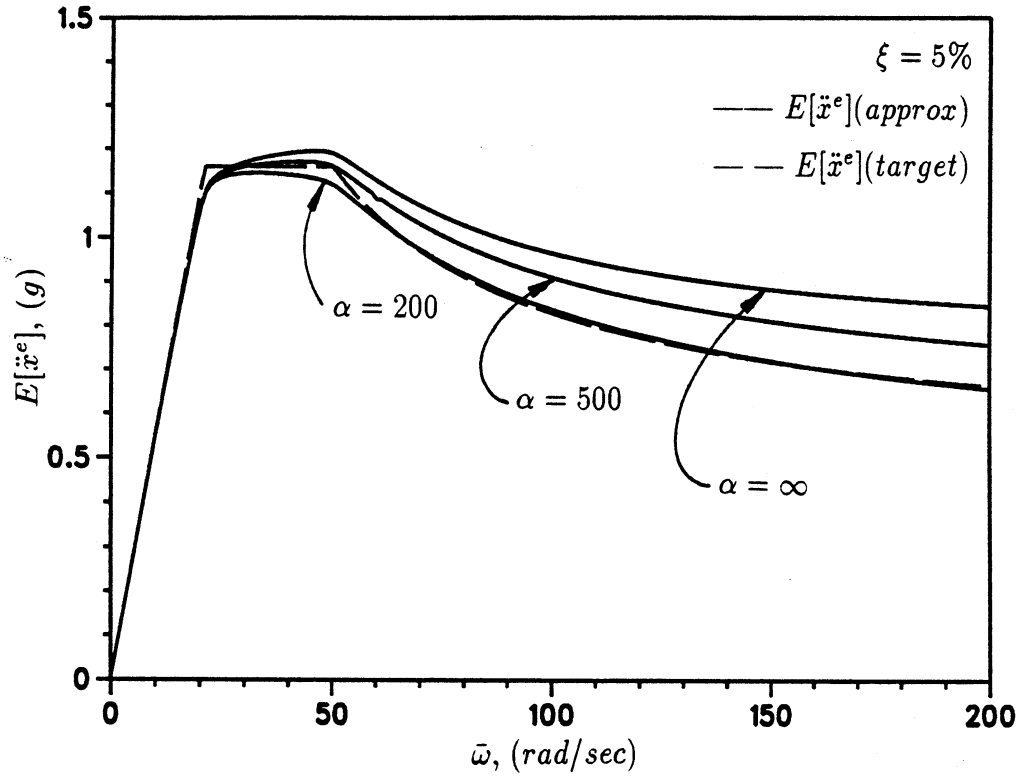

Fig. 2.4 *Matching of the response spectra based on (2.20) and (2.19)*

The iterative procedure which was described for evaluation of the coefficier ϕ was written in conjunction with (2.18). The same procedure is also applicat conjunction with (2.20) provided that α remains the same until an acceptable ϕ is reached. Supposing that α equals a large number, such as 10^5, ψ is practically equal to 1 for all frequencies of interest. The iterative procedure will therefore produce the same results as given in Table 2.1 and Fig. 2.3. To force $E[\ddot{x}^e](approx)$ to tend closer to $E[\ddot{x}^e](target)$ in Fig. 2.3, successively smaller values are assigned to α; each time

a new ϕ is obtained and $E[\ddot{x}^e](approx)$ tends closer to $E[\ddot{x}^e](target)$. This process is shown graphically in Fig. 2.4 in which the $E[\ddot{x}^e](approx)$ closest to $E[\ddot{x}^e](target)$ corresponds to

$$\alpha = 200 \quad b_1 = 5.2560 \quad b_2 = 1.2798 \quad c_1 = 1.3671 \quad c_2 = 2.5943$$

In this spectrum, the ordinates at frequencies 20.88 and 50 rad/sec have the largest nonconservative errors (of the order of 5%) with respect to the target spectrum. These frequencies define the range of fundamental frequencies of most low to medium rise building structures. Therefore it is appropriate to improve the correcting function ψ such that this portion of the response spectrum takes conservative values. This can be done without introducing any additional unknown parameters by redefining ψ as

$$\psi = \begin{cases} 1 + \frac{\omega_0}{\alpha} \; ; & \omega \leq \omega_0 \\ \left(1 + \frac{\omega_0}{\alpha}\right) exp\left(\frac{\omega_0 - \omega}{\alpha}\right) \; ; & \omega > \omega_0 \end{cases} \tag{2.21}$$

in which α remains the only unknown parameter to be determined through the same iterative procedure.

The final result is shown in Fig. 2.5 in which the approximate spectrum envelopes the target spectrum at all frequencies below 170 rad/sec. The largest conservative error is about 4% and occurs at a frequency around 30 rad/sec. Beyond 170 rad/sec the approximate spectrum falls slightly below the target spectrum. These frequencies are higher than normally encountered in building practice. The approximate spectrum of Fig. 2.5 corresponds to

$$\alpha = 150 \quad b_1 = 5.2418 \quad b_2 = 1.2814 \quad c_1 = 1.4816 \quad c_2 = 2.5657$$

With these values, rounded to two decimal places, and using (2.13), (2.17), and (2.21), (2.20) takes the following form

$$S_{\ddot{x}_b} = \begin{cases} \frac{g^2}{5\pi} \frac{1.14}{5.24+1.28ln(\omega)} \frac{\omega}{324} \; ; & 0.05 \leq \omega < 20.88 \\ \frac{g^2}{5\pi} \frac{1.14exp\left(\frac{20.88-\omega}{150}\right)}{1.48+2.57ln(\omega)} \frac{1.35}{\omega} \; ; & 20.88 \leq \omega < 50 \\ \frac{g^2}{5\pi} \frac{1.14exp\left(\frac{20.88-\omega}{150}\right)}{1.48+2.57ln(\omega)} \left(\frac{0.25}{\omega} + \frac{33}{\omega^2} + \frac{1089}{\omega^3}\right) \; ; & \omega \geq 50 \end{cases} \tag{2.22}$$

Note that the lowest value selected for ω is 0.05. This number is approximately the minimizer of the positive part of the function

$$\frac{\omega}{5.24 + 1.28ln(\omega)}$$

which appears in the first segment of (2.22). Such remedial measure is required since, as mentioned previously, $S_{\ddot{x}_b}$ is physically nonnegative and its first segment is an increasing function of ω. Should it be necessary, one can define a linear segment extending from the point $\{0,0\}$ to the point $\{0.05, S_{\ddot{x}_b}(0.05)\}$ and thus obtain a complete one-sided *psd* ranging from zero to infinity.

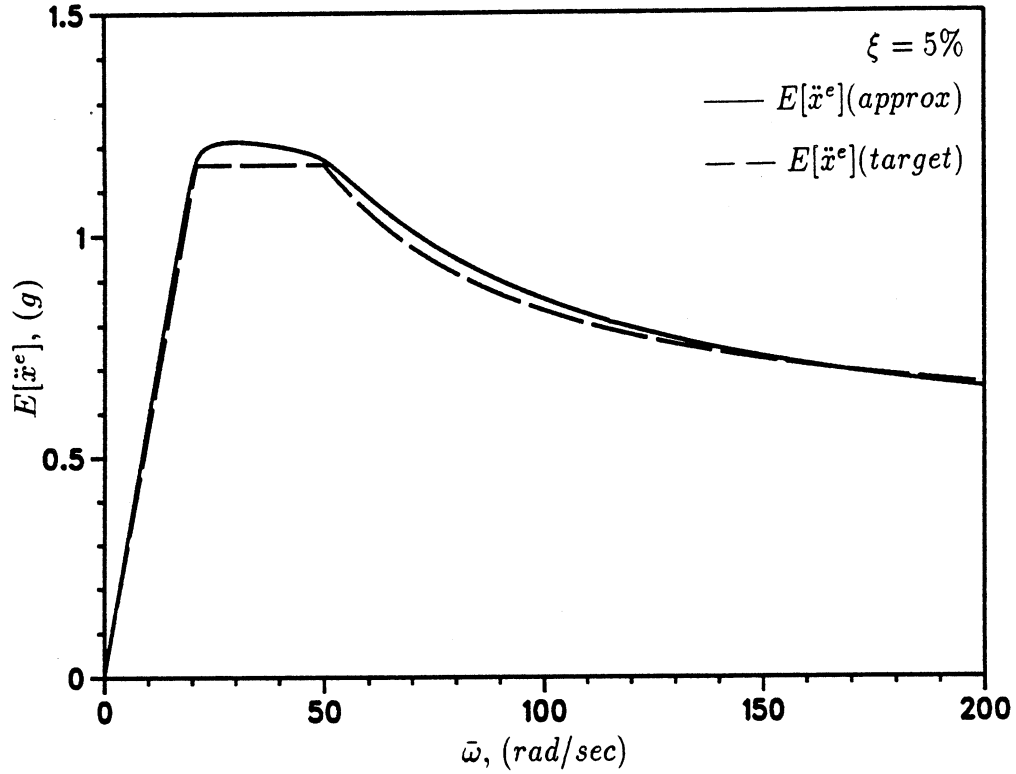

Fig. 2.5 *Matching of the response spectra based on (2.20) and (2.21)*

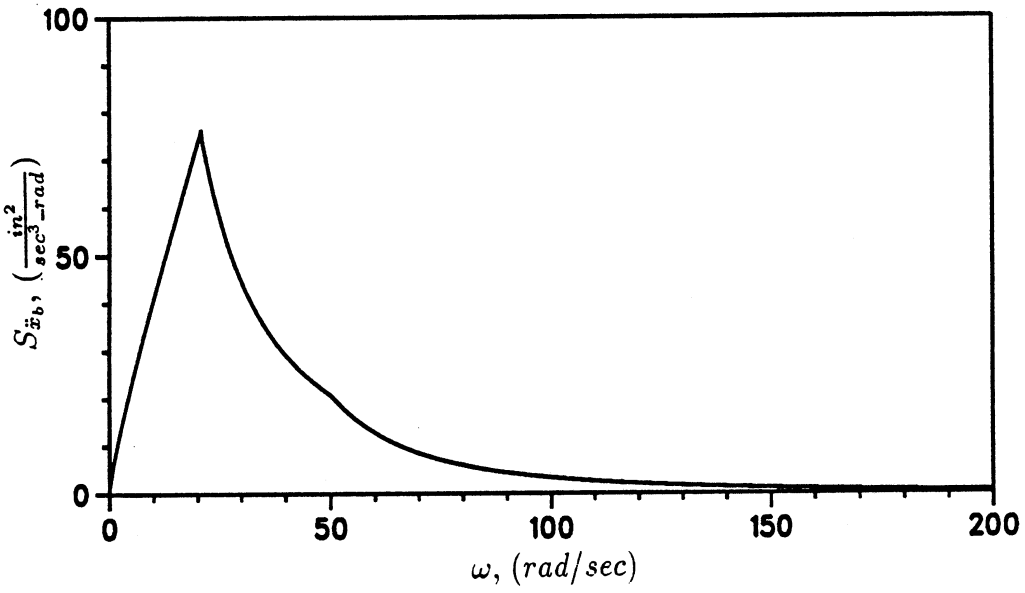

Fig. 2.6 *Spectrum-compatible psd function (2.22)*

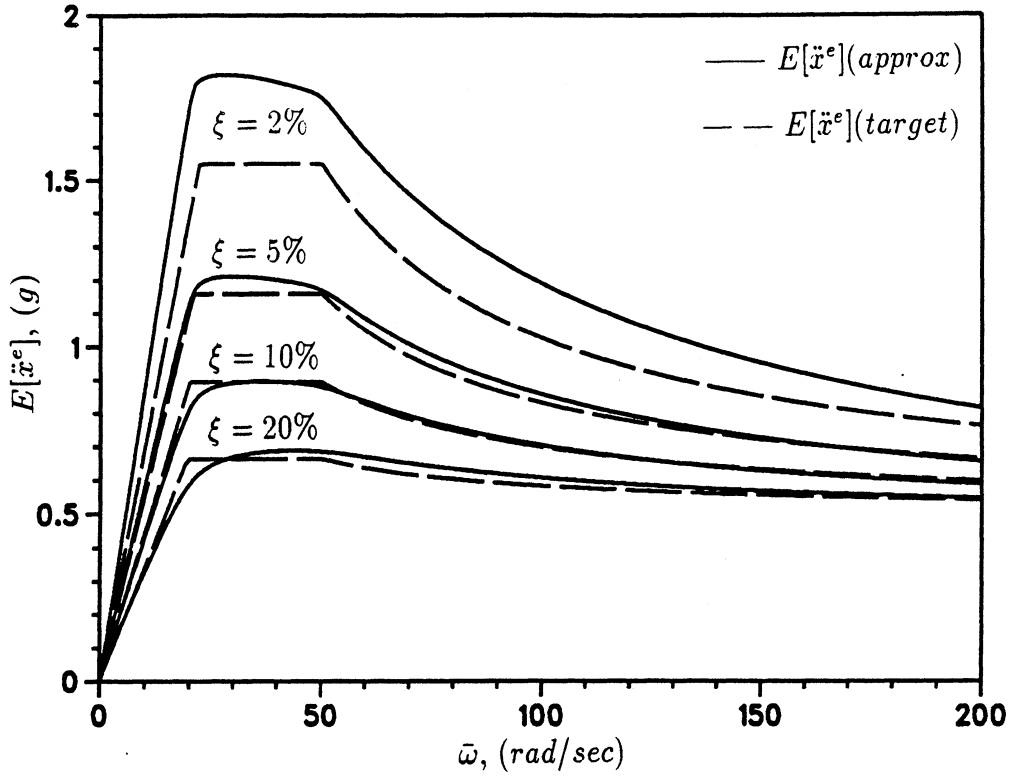

Fig. 2.7 *Approximate and target mean acceleration response spectra*

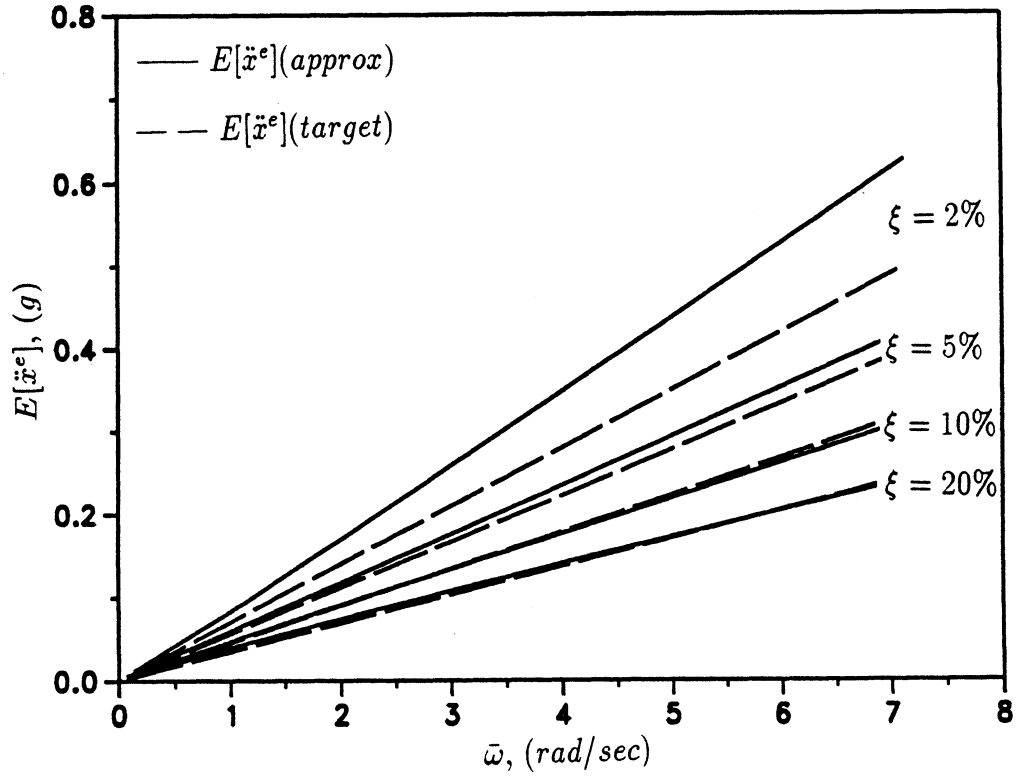

Fig. 2.8 *Low frequency portion of Fig. 2.7*

The excitation *psd* function represented by (2.22) is plotted in Fig. 2.6. It is a characterization of a magnitude 7.5 earthquake felt on rock deposits 10 *km* from the source of energy release. The family of response spectra shown in Fig. 2.1 also characterize the same earthquake excitation. In deriving (2.22), however, only the 5% response spectrum was used in the matching process. To have a broader range of applicability, (2.22) should also correspond to the response spectra with other damping values and hence have no or little dependence on damping.

In order to illustrate the extent of applicability of (2.22), this equation was used, together with (2.9), to generate a number of mean acceleration response spectra for different damping ratios. The results are shown in Fig. 2.7 and are identified as $E[\ddot{x}^e](approx)$. In the same figure, the response spectra of Fig. 2.1, identified as $E[\ddot{x}^e](target)$, are also shown for comparison. The low frequency portion of Fig. 2.7, which is of greater utility for modular structures, is redrawn in Fig. 2.8 for closer inspection. From these figures it can be noted that in addition to the response spectra with 5% damping, which were required to match, the response spectra with 10% and 20% damping are also in close agreement. The approximate 2% response spectrum is everywhere greater than the corresponding target spectrum, and hence is on the conservative side. The conservatism is most significant at intermediate frequencies.

On the basis of these findings, (2.22) is applicable to the analysis of structures with damping values between 5% to 20%. These values cover the range of damping widely believed to be present in conventional structures. The insignificant dependence of (2.22) on damping values of practical importance (5% to 20%) clearly shows applicability of (2.1), (2.3), and (2.9), and their associated underlying hypotheses to the earthquake excitation and response processes. In the probabilistic approach to response optimization of modular structures, which will be presented in the following chapter, the *psd* function given by (2.22) will be used as a characterization of the ground acceleration process.

2.4 Response Spectra for High Damping

As has been mentioned, the *psd* function (2.22) pertains to a particular category of earthquakes. Site-specific response spectrum statistics for dampings up to 20% are abundantly available (Mohraz and Elghadamsi, 1989). The same is not however true for large values of damping. Structures which are designed with supplemental mechanical dampers are likely to have dampings in excess of 20%. This will be the case in some of the optimal design illustrations in chapter 3 of which the most damped example has 73% damping.

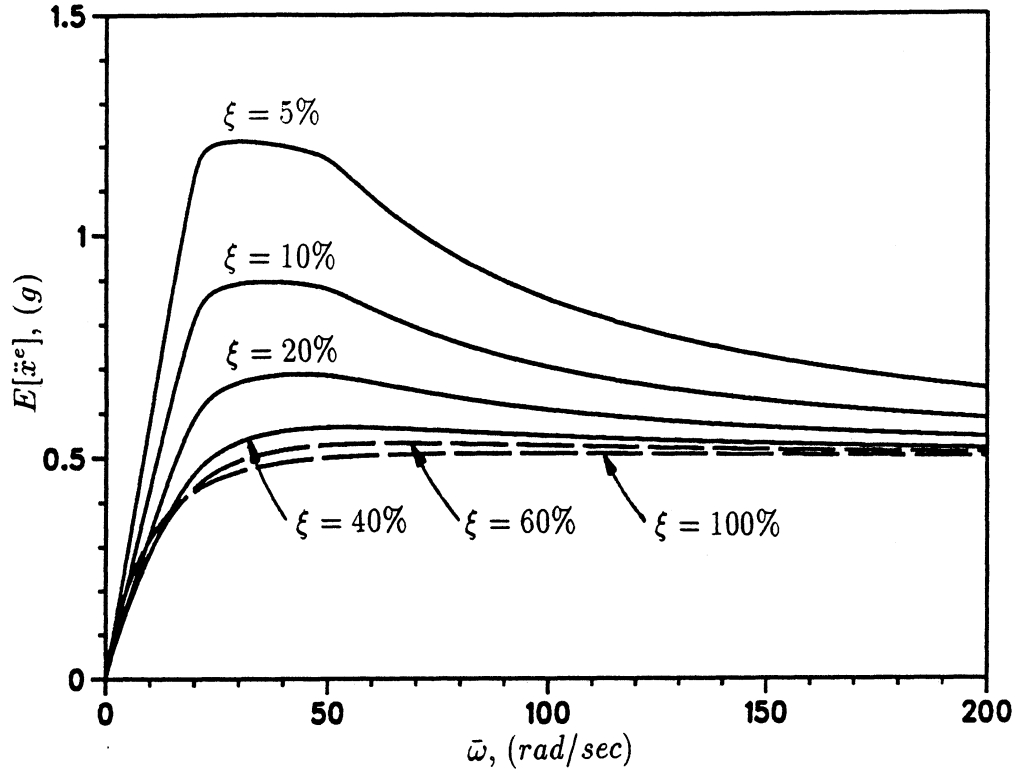

Fig. 2.9 *Mean acceleration response spectra derived from psd function (2.22*

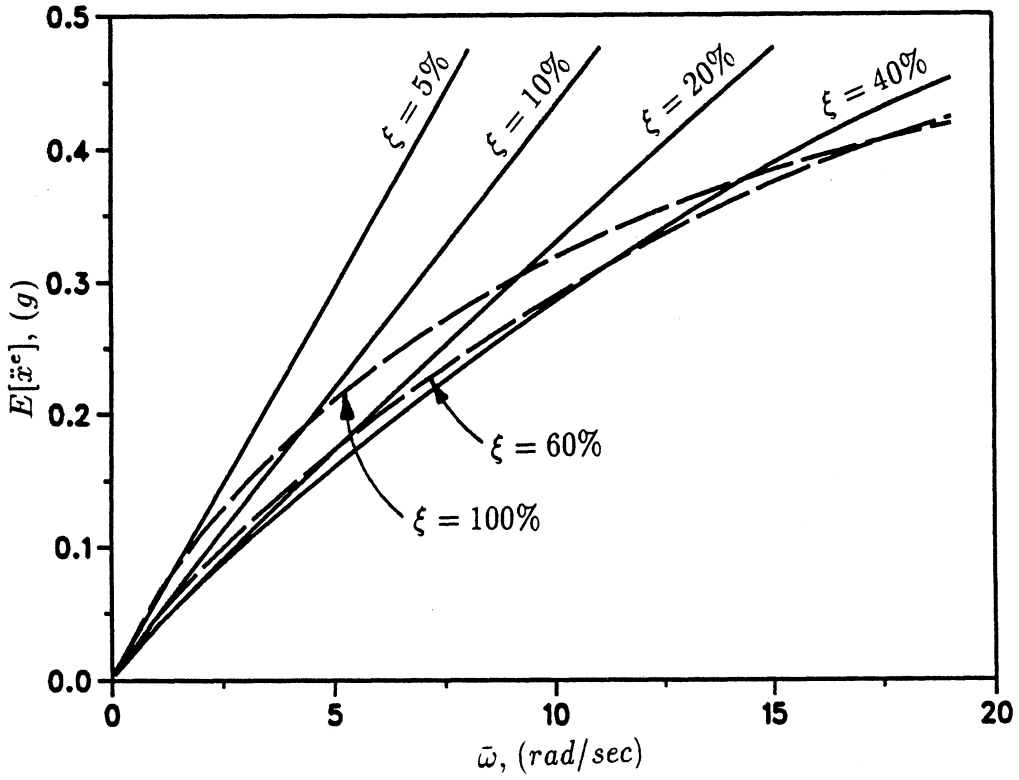

Fig. 2.10 *Low frequency portion of Fig. 2.9*

In the previous section the *psd* function (2.22) was shown to correspond to damping values of 5% to 20%. In the absence of site-specific response spectra for dampings in excess of 20%, this *psd* function will also be used for highly damped optimal design problems in Chapter 3. A qualitative justification for this is offered in the remainder of this section.

Table 2.2

Effect of high damping on acceleration response spectrum

	maximum acceleration response at π rad/sec (units: in/sec^2)		
earthquake records	*50% damping*	*100% damping*	*150% damping*
El Centro 1940 NS	45	55	70
Taft 1952 N69W	22	34	41
Gateway 1969	50	62	70

Fig. 2.9 serves to illustrate the general trend of the response spectra derived from the *psd* function (2.22) for dampings in the range of 5% to 100%. The low frequency portion of these spectra is shown in Fig. 2.10. From these figures it is seen that, in the intermediate to high frequency range, the effectiveness of damping vanishes at large values. Moreover, at low frequencies, increased damping has an adverse effect — it tends to increase the intensity of the acceleration response spectra. These same trends can be observed from the high damping acceleration response spectra computed by Ashour and Hanson (1987). They investigated the effect of up to 150% damping on the acceleration response spectra of three actual earthquakes[2]. In order to provide an example, the information collected in Table 2.2 was extracted from their graphical results at a frequency of π *rad/sec* (period of 2 *sec*). It can be seen that, at this low frequency and for high damping ratios, increased damping results in increased acceleration for all earthquakes considered.

[2]El Centro 1940 NS, Taft 1952 N69W, and Gateway 1969

CHAPTER 3

THE OPTIMAL DESIGN PROBLEMS

3.1 Introduction

In Chapter 1 essential features of a modular structure were described. It was pointed out that a base isolated structure is a special case of a modular structure in which the control elements are placed at the base. It was also noted that placement of the control elements at a higher level isolates the top portion from the bottom, and thus provides a classic case of vibration isolation.

A method of deriving a *psd* of excitation $S_{\ddot{x}_b}$ compatible with site-specific design response spectra was developed in Chapter 2. It was shown that the mean $E[z^e]$ and the standard deviation σ_{z^e} of the extreme values z^e of any response process z can be found by a knowledge of $S_{\ddot{x}_b}$ and the complex frequency response H_z associated with z.

In this chapter the complex frequency response functions of various response quantities for one and two degree of freedom systems are derived. These functions together with $S_{\ddot{x}_b}$ as given by (2.22) are required to compute $E[z^e]$ and σ_{z^e} for any response process z. Knowledge of $E[z^e]$ and σ_{z^e} will then facilitate formulation of the design optimization problems.

The subsequent interest in this chapter is to compare the performance of a one degree of freedom base isolated structure to that of a two degree of freedom modular version. It is clear that the choice between base isolation and modular schemes should be based on either the most favorable response under equal resource availability; or the least resource consumption for the same level of response. Consequently, following the optimal design formulations, a discussion on the equivalence of resources used in each problem is presented. It will be shown that a practically meaningful comparison requires a detailed cost analysis relative to each competing design option. Without access to actual cost data, a volumetric material analysis will be conducted in the context of a specific example with the result that, for the same level of response, the

control elements in the modular structure require less material than those in the base isolated structure. From a practical standpoint however it will be argued that, for the same level of response induced by earthquakes on *rock deposits*, the construction of a base isolated system will be relatively less costly. It is however well established that, on soft soil deposits, the dominant periods of earthquakes, such as the one which occurred in Mexico City in 1985, will be in the range of the fundamental periods practically achievable in base isolated structures (Seed, Ugas, and Lysmer, 1976; Mayes, 1989). Since with a modular scheme even longer fundamental periods can be attained, it is conceivable that modular structures can be designed to perform favorably in earthquakes filtered through soft soil deposits.

Next, attention will be turned to specific applications of a modular structure. In this regard two possibilities will be explored. Firstly, situations may arise in which, because of the practical limits on the extent of flexibility and lateral displacement of a base isolation system, the desired response reduction cannot be achieved. In such cases a modular structure with two levels of control elements can result in the desired response reduction. In this context, it will be shown that a modular design can effectively utilize damping as high as practically possible, while the same levels of damping in a base isolated design will have an adverse effect on the quality of response. Secondly, as a more significant application, the effectiveness of a modular solution in retrofitting buildings with soft first stories will be demonstrated.

3.2 One Degree of Freedom Systems

A low to medium rise base isolated structure can be idealized by a one degree of freedom *(1dof)* model in which a lumped mass m is connected to a moving base by means of a linear spring of constant k and a viscous damper of constant c. In this model k and c represent, respectively, the lateral stiffness and the damping coefficient of the control elements on which the structure stands; and m represents the total mass of the structure. The total mass is assumed to be unaffected by the relatively small mass of the control elements. The motion of the base is given in terms of its acceleration $\ddot{x}_b$.

In a *1dof* system the response quantities, which are of significance for design, are the relative displacement $y = x - x_b$, and the interstory shear forces which can be written in terms of the absolute acceleration of the mass $\ddot{x}$. The differential equation of motion in terms of the relative displacement y is

$$m\ddot{y} + c\dot{y} + ky = -m\ddot{x}_b \tag{3.1}$$

Once the relative displacement y is evaluated from this equation the absolute acceleration of the mass $\ddot{x}$ is found by substituting $\ddot{y} = \ddot{x} - \ddot{x}_b$ in (3.1):

$$m\ddot{x} = -c\dot{y} - ky \tag{3.2}$$

The complex frequency responses H_y, and $H_{\ddot{x}}$, associated with y, and $\ddot{x}$, respectively, are obtained by substituting

$$\ddot{x}_b = exp(i\omega t) \tag{3.3}$$

$$y = H_y \ddot{x}_b \tag{3.4}$$

$$\ddot{x} = H_{\ddot{x}} \ddot{x}_b \tag{3.5}$$

in (3.1) and (3.2):

$$H_y = \frac{-m}{k - m\omega^2 + ic\omega} \tag{3.6}$$

$$H_{\ddot{x}} = \frac{k + ic\omega}{k - m\omega^2 + ic\omega} \tag{3.7}$$

The shear force at the base is $V = c\dot{y} + ky$. Using (3.2) it can be written as

$$V = -m\ddot{x} \tag{3.8}$$

The complex frequency response, H_V, associated with V is obtained by substituting $V = H_V \ddot{x}_b$ and (3.5) in (3.8):

$$H_V = -mH_{\ddot{x}} \tag{3.9}$$

which upon using (3.7) becomes

$$H_V = \frac{-m(k + ic\omega)}{k - m\omega^2 + ic\omega} \tag{3.10}$$

For future reference the natural frequency, $\bar{\omega}$, and the damping ratio, ξ, of a *1dof* system are defined as follows

$$\bar{\omega}^2 = \frac{k}{m}; \qquad \xi = \frac{c}{2m\bar{\omega}}$$

3.3 Two Degree of Freedom Systems

Modular structures can be modeled as lumped parameter systems in which one or more stories can be regarded as a single module. Because of high lateral stiffness, each module is considered infinitely rigid and therefore can be represented by a single mass. The coupling of the modules is accomplished through the control elements with

specified stiffness and damping properties. The behavior of a two degree of freedom *(2dof)* system subjected to base excitation would therefore correspond to that of a low to medium rise modular structure with control elements placed at the base and at one other location between adjacent stories.

Consider a *2dof* system with masses m_1 and m_2; spring constants k_1 and k_2; and viscous damping coefficients c_1 and c_2. In this model m_1 is the total mass of the module above the base; m_2 is the total mass of the module above m_1; k_1 and c_1 represent, respectively, the lateral stiffness and the damping coefficient of the control elements placed between the base and m_1; and k_2 and c_2 represent, respectively, the lateral stiffness and the damping coefficient of the control elements placed between m_1 and m_2. The motion of the base in this case, as in the case of the *1dof* system, is also given in terms of its acceleration $\ddot{x}_b$. Let x_b, x_1, and x_2 denote the absolute displacements of the base, the mass m_1, and the mass m_2, respectively. The coupled differential equations of motion for this system can be written in terms of the relative displacements $y_1 = x_1 - x_b$ and $y_2 = x_2 - x_1$ as follows

$$m_1\ddot{y}_1 + c_1\dot{y}_1 + k_1y_1 - c_2\dot{y}_2 - k_2y_2 = -m_1\ddot{x}_b \tag{3.11}$$

$$m_2(\ddot{y}_1 + \ddot{y}_2) + c_2\dot{y}_2 + k_2y_2 = -m_2\ddot{x}_b \tag{3.12}$$

in which the response quantities y_1 and y_2 are related to the base acceleration $\ddot{x}_b$. The other response quantities of interest are the absolute acceleration of the masses $\ddot{x}_1$ and $\ddot{x}_2$. These quantities are obtained by substituting $\ddot{y}_1 = \ddot{x}_1 - \ddot{x}_b$ and $\ddot{y}_2 = \ddot{x}_2 - \ddot{x}_1$ in (3.11) and (3.12):

$$m_1\ddot{x}_1 = -c_1\dot{y}_1 - k_1y_1 + c_2\dot{y}_2 + k_2y_2 \tag{3.13}$$

$$m_2\ddot{x}_2 = -c_2\dot{y}_2 - k_2y_2 \tag{3.14}$$

The shear force at any level can be written as a linear combination of the accelerations $\ddot{x}_1$ and $\ddot{x}_2$.

Associated with the four response quantities y_1, y_2, $\ddot{x}_1$, and $\ddot{x}_2$, there are four complex frequency response functions which are respectively denoted as H_{y_1}, H_{y_2}, $H_{\ddot{x}_1}$, and $H_{\ddot{x}_2}$. Making the substitutions

$$y_1 = H_{y_1}\ddot{x}_b \tag{3.15}$$

$$y_2 = H_{y_2}\ddot{x}_b \tag{3.16}$$

and (3.3) into (3.11) and (3.12):

$$H_{y_1} = \frac{m_1m_2\omega^2 - (m_1 + m_2)k_2 - i(m_1 + m_2)c_2\omega}{\Delta} \tag{3.17}$$

$$H_{y_2} = \frac{-m_2 k_1 - i m_2 c_1 \omega}{\Delta} \tag{3.18}$$

in which

$$\begin{aligned} \Delta &= m_1 m_2 \omega^4 - [m_2 k_1 + (m_1 + m_2) k_2 + c_1 c_2] \omega^2 + k_1 k_2 \\ &- i\{[(m_1 + m_2) c_2 + m_2 c_1] \omega^3 - (k_1 c_2 + k_2 c_1) \omega\} \end{aligned} \tag{3.19}$$

Substituting

$$\ddot{x}_1 = H_{\ddot{x}_1} \ddot{x}_b \tag{3.20}$$

$$\ddot{x}_2 = H_{\ddot{x}_2} \ddot{x}_b \tag{3.21}$$

(3.15), and (3.16) into (3.13) and (3.14):

$$m_1 H_{\ddot{x}_1} = -(k_1 + i c_1 \omega) H_{y_1} + (k_2 + i c_2 \omega) H_{y_2} \tag{3.22}$$

$$m_2 H_{\ddot{x}_2} = -(k_2 + i c_2 \omega) H_{y_2} \tag{3.23}$$

which upon using (3.17) and (3.18) lead to

$$H_{\ddot{x}_1} = \frac{-(m_2 k_1 + c_1 c_2) \omega^2 + k_1 k_2 - i\left[m_2 c_1 \omega^3 - (k_1 c_2 + k_2 c_1) \omega\right]}{\Delta} \tag{3.24}$$

$$H_{\ddot{x}_2} = \frac{-c_1 c_2 \omega^2 + k_1 k_2 + i(k_1 c_2 + k_2 c_1) \omega}{\Delta} \tag{3.25}$$

The shear force at the base is $V_1 = c_1 \dot{y}_1 + k_1 y_1$ and the shear force between m_1 and m_2 is $V_2 = c_2 \dot{y}_2 + k_2 y_2$. Using (3.13) and (3.14) these response quantities can be written in terms of the acceleration of the masses $\ddot{x}_1$ and $\ddot{x}_2$:

$$V_1 = -m_1 \ddot{x}_1 - m_2 \ddot{x}_2 \tag{3.26}$$

$$V_2 = -m_2 \ddot{x}_2 \tag{3.27}$$

The complex frequency responses H_{V_1} and H_{V_2}, associated with V_1 and V_2, respectively, are obtained by substituting

$$V_1 = H_{V_1} \ddot{x}_b \tag{3.28}$$

$$V_2 = H_{V_2} \ddot{x}_b \tag{3.29}$$

(3.20) and (3.21) into (3.26) and (3.27):

$$H_{V_1} = -m_1 H_{\ddot{x}_1} - m_2 H_{\ddot{x}_2} \tag{3.30}$$

$$H_{V_2} = -m_2 H_{\ddot{x}_2} \tag{3.31}$$

which upon using (3.24) and (3.25) become

$$H_{V_1} = \frac{\left[\begin{array}{c}[m_1m_2k_1 + (m_1+m_2)c_1c_2]\,\omega^2 - (m_1+m_2)k_1k_2 \\ +i\,[m_1m_2c_1\omega^3 - (m_1+m_2)(k_1c_2+k_2c_1)\omega]\end{array}\right]}{\Delta} \tag{3.32}$$

$$H_{V_2} = \frac{m_2c_1c_2\omega^2 - m_2k_1k_2 - im_2(k_1c_2+k_2c_1)\omega}{\Delta} \tag{3.33}$$

In the presentation of results which appear in later sections, reference will be made to the modal frequencies, ω_1 and ω_2, and the modal damping ratios, ξ_1 and ξ_2. These quantities are defined in Appendix B where, for the cases of nonproportional damping, a procedure for their evaluation is presented.

3.4 The Formulation of Design Problems

In a structural optimization problem the concern is to minimize an objective function over a prescribed design space. The objective function is a measure of the cost or the reliability of the structure; both of which can be represented in terms of one or several of the response quantities related to various parts of the structure. The design space is defined by a set of constraints placed on the design variables; and on those response quantities which do not explicitly appear in the objective function.

The computational algorithm, used for solving the nonlinear optimization problems in this research, is based on a gradient projection technique devised by Haug and Arora (1979). This algorithm was coded into a computer program and verified by solving several nonlinear programming problems with known solutions. The algorithm, a brief theoretical background, and one verification problem can be found in Appendix A.

The response quantities which appear in the subsequent optimal design problems are written in terms of their extreme value statistics. These statistics were formulated in Chapter 2 using a general response quantity z. In particular (2.6) and (2.7) provide, respectively, the mean $E[z^e]$ and the standard deviation σ_{z^e} of the extreme values z^e related to the response quantity z. In the process of computing these statistics, H_z corresponds to the appropriate complex frequency response functions which were derived in the previous sections. In every instance $S_{\ddot{x}_b}$, the ground acceleration *psd*, is given by (2.22). This *psd* function is a characterization of a magnitude 7.5 earthquake recorded on rock deposits 10 *km* from the source.

The probability distribution function, $P(z_0)$, signifying the probability that z^e is less than a symmetric barrier level $\pm z_0$, is given by (2.3). A desired barrier level for

the extreme value of a response quantity can be written as the sum of its mean value and some multiple β of its standard deviation. The probability of not exceeding this barrier level can then be computed from (2.3). A lower bound to this probability can be established using Chebyshev's inequality (Nigam, 1983):

$$P(E[z^e] + \beta\sigma_{z^e}) \geq 1 - \frac{1}{\beta^2} \tag{3.34}$$

in which the left hand side means the probability that z^e is less than $E[z^e] + \beta\sigma_{z^e}$. Unless otherwise noted, $\beta = 4$ will be used in all the subsequent problems. This value, according to (3.37), corresponds to about 94% probability that z^e will not be exceeded.

Drawing upon the preceding discussions, the remainder of this section serves to formulate the optimal design problems. First, a formulation is presented for the *2dof* modular models whose mass distributions, m_1 and m_2, were summarized in Table 1.2 of Section 1.3. Next, a formulation is given for the *1dof* base isolated model whose mass m equals the sum $m_1 + m_2$. Following the two optimal design formulations attention will be focused on whether, with the same resource availability, any one of the *2dof* modular models will perform more favorably than the *1dof* base isolated model.

For a *2dof* modular structure the variables of the optimization problem are the stiffness k_1 and the damping coefficient c_1 of the control elements placed at the base; and the stiffness k_2 and the damping coefficient c_2 of the control elements placed at a higher level. The task is therefore to find the control element parameters k_1, c_1, k_2, and c_2 which correspond to the following minimization problem:

$$\begin{array}{ll} \textit{minimize} & E[V_1^e] \\ \textit{such that} & y_1^e \leq y_1^u \\ & y_2^e \leq y_2^u \\ & k_1 \geq k_1^l \\ & k_2 \geq k_1^l \\ & c_1 \leq c_1^u \\ & c_2 \leq c_2^u \end{array} \tag{3.35}$$

in which

$$\begin{aligned} y_1^e &= E[y_1^e] + \beta\sigma_{y_1^e} \\ y_2^e &= E[y_2^e] + \beta\sigma_{y_2^e} \end{aligned}$$

and the superscripts l and u mean, respectively, lower and upper bounds on the corresponding quantities. In this formulation the objective function is the mean

extreme value of the base shear V_1 and reflects a measure of the building cost ascribed to earthquake protection. The constraints on the displacement, stiffness, and damping of the control elements can be considered as measures of the available resources.

For a *1dof* base isolated structure an optimal design can be posed as finding the control element parameters k and c corresponding to the following minimization problem:

$$\begin{array}{ll} \textit{minimize} & E[V^e] \\ \textit{such that} & y^e \leq y^u \\ & k \geq k^l \\ & c \leq c^u \end{array} \tag{3.36}$$

in which

$$y^e = E[y^e] + \beta\sigma_{y^e}$$

In this formulation, also, the objective function is the mean extreme value of the base shear V and the constraints reflect a measure of the available resources.

3.5 The Problem of Equivalence of Resources

In both problems, (3.35) and (3.36), the objectives are the same. The damping constraints in (3.35), owing to the use of viscous dashpots in the equilibrium equations, can be combined into a single constraint

$$c_1 + c_2 \leq c^u$$

which is equivalent to the damping constraint in (3.36). Beyond this, in the framework of the present formulation, no equivalence in resources can be readily established. In the discussion on the design of rubber bearings in Section 1.4 it was pointed out that as the axial load and the vertical stiffness demand on the bearings increase, it will be increasingly more costly to satisfy the requirements for lateral stiffness, lateral displacement, and the safety against buckling. Therefore the cost of a control element design simultaneously depends on its lateral stiffness, its allowable displacement, and the level at which it is installed. At the base, the requirements for the vertical stiffness, shearing strain, and safety against buckling are more stringent than, for instance, at the roof level. Furthermore, while laminated rubber bearings are commonly used at the base of structures, they may not be the most economical choice for the control elements at the roof level where the axial load is relatively small and a variety of other conceivable *soft spring* mechanisms can be used.

The two optimal design problems (3.35) and (3.36), although independently adequate for preliminary investigations, are not in the form suitable for comparative studies. This is also true regarding comparisons among the various *2dof* models sharing the same formulation (3.35). What can be done however is to perform, for instance, the comparative studies in two steps:

1. Solve the optimal design of the *1dof* model with given displacement and damping resources and then, using the same damping resource, solve for the optimal design of the *2dof* model using a displacement resource which produces the same objective as in the *1dof* case.

2. Having the displacements and stiffness values, design the control elements for both cases and compare their costs.

To illustrate, consider the following optimal design problems. For the *1dof* base isolated model with $m = 350$ *kip-mass*,

$$\begin{aligned} \textit{minimize} \quad & E[V^e] \\ \textit{over} \quad & k, c \\ \textit{such that} \quad & y^e \leq 9.6 \ in \\ & c \leq 0.365 \ kip\_sec/in \\ & k \geq 1 \ kip/in \end{aligned} \tag{3.37}$$

and for the *2dof* modular model with $m_1 = 300$ *kip-mass* and $m_2 = 50$ *kip-mass*,

$$\begin{aligned} \textit{minimize} \quad & E[V_1^e] \\ \textit{over} \quad & k_1, k_2, c_1, c_2 \\ \textit{such that} \quad & y_1^e + y_2^e \leq 13 \ in \\ & c_1 + c_2 \leq 0.365 \ kip\_sec/in \\ & c_1 \geq 0.001 \ kip\_sec/in \\ & c_2 \geq 0.001 \ kip\_sec/in \\ & k_1 \geq 1 \ kip/in \\ & k_2 \geq 1 \ kip/in \end{aligned} \tag{3.38}$$

In these problems, the objectives and the damping resources are the same while the displacement resources are different. These resources have been so selected to produce practically equal objectives and to result in approximately 5% damping in the *1dof* model. The bound on the stiffness value in problem (3.37) and the bounds on the individual stiffness and damping values in problem (3.38) are precautionary and will turn out to have no effect on the outcome. The solutions, *i.e.* the stiffness

and damping coefficients, together with other pertinent information are summarized in Table 3.1.

Table 3.1

Optimal design solutions to problems (3.37) and (3.38)

2dof system			*1dof system*		
units	*quantity*	*value*	*value*	*quantity*	*units*
kips	$E[V_1^e]$	83.92	83.42	$E[V^e]$	*kips*
kip/in	k_1	30.73	14.88	k	*kip/in*
kip/in	k_2	3.58	–	–	–
kip-sec/in	$c_1 + c_2$	0.365	0.365	c	*kip-sec/in*
kip-sec/in	c_1	0.046	–	–	–
kip-sec/in	c_2	0.319	–	–	–
in	$y_1^e + y_2^e$	13	9.60	y^e	*in*
in	y_1^e	4.44	–	–	–
in	y_2^e	8.56	–	–	–
g	$E[\ddot{x}_1^e]$	0.26	0.24	$E[\ddot{x}]$	*g*
g	$E[\ddot{x}_2^e]$	0.40	–	–	–
rad/sec	ω_1	6.79	4.05	$\bar{\omega}$	*rad/sec*
rad/sec	ω_2	4.87	–	–	–
–	ξ_1	0.12	0.05	ξ	–
–	ξ_2	0.14	–	–	–
kip-mass	$m_1 + m_2$	350	350	m	*kip-mass*
kip-mass	m_1	300	–	–	–
kip-mass	m_2	50	–	–	–

Note that the resources are fully consumed in both problems. This implies that any decrease in resources will cause the objectives to increase. In particular, decreasing the displacement resource of the modular model (13 *in*) to that of the base isolated model (9.6 *in*) will increase the objective from 83.92 *kips* to 124.02 *kips*. At first, this indicates that for equal total damping and displacement the base isolated model is more favorable than the modular model. Further evaluation of the physical design of the control elements will however provide competing arguments for both structural systems. To this end, let the control elements used in both structures be of the type

described in Section 1.4. The required design equations (1.12), (1.18), and (1.19) are repeated here, respectively, for convenience:

$$K_l = \frac{\pi G R^2}{n h_r} \tag{3.39}$$

$$P_c = \frac{\sqrt{2}\pi R^2}{4 h_r} K_l \tag{3.40}$$

$$K_v = \frac{3R^2}{2h_r^2} K_l \tag{3.41}$$

where, as before, K_l is the lateral stiffness equal to k_1, k_2, or k as given in Table 3.1; P_c is the critical buckling load; K_v is the vertical stiffness; G is the shear modulus of the rubber material; R and h_r are, respectively, the radius and thickness of the rubber sheets; and n is the number of rubber sheets used in the laminated construction of the bearing.

A consistent design procedure requires that the shearing strain $\frac{\delta}{nh_r}$, resulting from lateral displacement δ, the ratio $\frac{R}{h_r}$, and the shear modulus G be the same for all designs. Assuming $\frac{\delta}{nh_r} = 50\%$ and noting that δ is equal to y_1^e, y_2^e, or y^e in Table 3.1, the total thickness of rubber nh_r becomes known. Since K_l is also known for each case, with the assumption that $G = 200$ *psi*, (3.39) can be used to compute R. Setting the ratio $\frac{R}{h_r} = 45$, the rubber sheet thickness in each case can then be evaluated. subsequently, the number of rubber layers n becomes known. Finally (3.40) and (3.41) can be used to compute the buckling load P_c and the vertical stiffness K_v for each design. Of course when the values for P_c and K_v are not satisfactory, a smaller h_r, based on either (3.40) or (3.41), can be selected.

Using the above procedure, the control elements required for both models were designed. The results are summarized in Table 3.2. It should be noted that the dimensions for R and h_r, and the values for n (an integer) should be adjusted to obtain practical values. For the purpose of the present discussion, however, these values are kept unadjusted. From this data, it is clear that the resources used in the design of the control elements for the *2dof* model are substantially less than what is required for the *1dof* model. In particular, the volume of rubber material, vol_r, and the volume of steel material, vol_s, used in the *2dof* model are, respectively, 37% and 13% less than those in the *1dof* model. Also of interest is to note that both the vertical stiffness and the buckling load of the base control element in the *2dof* case are more than twice as large compared to those in the *1dof* model.

Although for the same base shear the modular structure requires less material resources for the control elements, the reduction is not sufficiently radical to offset

the costs associated with installation of a second level of control elements. From a practical point of view, it therefore appears that the construction cost of a base isolated structure, designed for earthquakes on rock deposits, will be relatively less. However, as will be shown in the remainder of this chapter, in certain situations, the modular structure can be considered as a viable alternative for earthquake resistant design.

Table 3.2

Control element designs for 1dof and 2dof systems(1)

quantity (units)	K_l *(kip/in)*	R *(in)*	h_r *(in)*	n *(-)*	vol_r(2) (ft^3)	vol_s(3) (ft^3)	K_v *(kip/in)*	P_c *(kips)*
1dof, base	14.88	21.32	0.48	40.27	15.9	$33.3h_s$(4)	44,640	15,755
2dof, base	30.73	20.84	0.47	19.06	7.0	$15.1h_s$	92,190	31,852
2dof, roof	3.58	9.88	0.22	78.00	3.0	$13.8h_s$	1,767	10,874
2dof, sum	–	–	–	–	10.0	$28.9h_s$	–	–
2dof, saving	–	–	–	–	37%	13%	–	–

(1) *Dimensions for R and h_r, and the values for n (an integer) should be adjusted to obtain practical values. For the purpose of the present discussion, however, these values are kept unadjusted.*

(2) *vol_r = volume of rubber*

(3) *vol_s = volume of steel*

(4) *h_s = thickness of each steel plate*

3.6 Specific Applications of a Modular Structure

From the numerical examples presented in the preceding section the following observations can be made:

1. For the same base shear, the control elements required for the base isolated structure are laterally more flexible than those needed at the base of the modular structure.

2. The vibration isolation action of the second mass in the modular structure effectively reduces the base displacement.

In the first instance, because of the practical limits on the extent of the lateral flexibility of the control elements in a base isolated structure, the modular scheme can

be viewed as a method to further improve the response without additional reduction in lateral flexibility at the base. For this reason, it is of interest to investigate the effect of mass distribution and damping on the optimal design of various *2dof* modular models which were described in Section 1.3. This task will be dealt with in the following section.

In the second instance, the vibration isolation action of the second mass in a *2dof* modular structure can be used to retrofit existing seismically hazardous buildings. In particular this idea can be applied to rigid multistory structures with soft first stories. This possibility will be studied in Section 3.8.

3.7 Effect of Mass Distribution and Damping

The effect of mass distribution and damping will be studied through specific examples. The term mass distribution refers to the proportion of the total mass of the building assigned to the lumped masses m_1 and m_2 of the corresponding *2dof* models. These models, resulting from the different alternatives in the location of the second level of control elements, were discussed in Section 1.3.

To study the effect of mass distribution, consider the following optimization problem:

$$\begin{aligned}
&given && m_1, m_2 \\
&minimize && E[V_1^e] \\
&over && k_1, k_2, c_1, c_2 \\
&such\ that && y_1^e \leq 6\ in \\
& && y_2^e \leq 6\ in \\
& && c_1 + c_2 \leq 1\ kip_sec/in \\
& && c_1 \geq 0.01\ kip_sec/in \\
& && c_2 \geq 0.01\ kip_sec/in \\
& && k_1 \geq 1\ kip/in \\
& && k_2 \geq 1\ kip/in
\end{aligned} \tag{3.42}$$

The results for six different mass ratios m_2/m_1 are summarized in Table 3.3. The mass ratio varies from 1/6 in case 1 to 6/1 in case 6 in increasing order. In all cases the total damping $c_1 + c_2$ and the maximum displacement y_2^e are at their upper limits. For all possible mass ratios, the expected value of the maximum base shear $E[V_1^e]$ is practically unchanged, ranging from 49 to 56 *kips*. However, the effect of mass ratio

on the base displacement and the stiffness coefficients is significant. With increasing mass ratio the base displacement y_1^e decreases while both stiffness coefficients k_1 and k_2 increase.

Table 3.3

Effect of mass distribution

units	*quantity*	*case 1*	*case 2*	*case 3*	*case 4*	*case 5*	*case 6*
–	m_2/m_1	1/6	2/5	3/4	4/3	5/2	6/1
kip-mass	$m_1 + m_2$	350	350	350	350	350	350
kip-mass	m_1	300	250	200	150	100	50
kip-mass	m_2	50	100	150	200	250	300
kip-sec/in	$c_1 + c_2$	1	1	1	1	1	1
kip-sec/in	c_1	0.50	0.15	0.01	0.01	0.01	0.01
kip-sec/in	c_2	0.50	0.85	0.99	0.99	0.99	0.99
rad/sec	ω_1	4.42	5.79	7.11	9.50	13.54	25.74
rad/sec	ω_2	3.84	3.79	3.40	3.36	3.45	3.53
–	ξ_1	0.44	0.26	0.21	0.18	0.16	0.16
–	ξ_2	0.16	0.24	0.21	0.17	0.14	0.14
kips	$E[V_1^e]$	53	54	49	49	53	56
in	y_1^e	6	4.5	3.6	2.7	2.1	1.1
in	y_2^e	6	6	6	6	6	6
kip/in	k_1	14.5	19.7	21.8	28.1	38.2	75.6
kip/in	k_2	2.0	4.1	5.4	7.3	9.6	11.0

The optimal designs in Table 3.3 can be viewed as possible options for further response improvement of a base isolated solution. The need for these options can arise in base isolation projects in which, because of high axial loads, the design of a particular device with a low enough lateral stiffness or a large enough allowable displacement becomes impractical. In this sense, the modular models in cases 1, 2, and 3, in which the second level of control elements carry relatively smaller axial loads, are most likely to succeed.

An interesting characteristic of a *2dof* modular structure is its capacity to admit very large amounts of damping. With fixed stiffness coefficients k_1 and k_2, the structure will effectively consume increasing levels of damping in order to reduce the base shear. The same is not true in a *1dof* base isolated structure. In this case,

given a fixed value for the stiffness k, the base shear tends to decrease with increasing damping; attains a minimum at an optimum damping value; and begins to increase as the damping further increases. To illustrate, consider the following optimal design problems. For a *1dof* system with $m = 350$ *kip-mass*,

$$\begin{aligned} \textit{minimize} \quad & E[V^e] \\ \textit{over} \quad & k, c \\ \textit{such that} \quad & y^e \leq 2 \ in \\ & c \leq 10 \ kip\_sec/in \\ & k \geq 50 \ kip/in \end{aligned} \tag{3.43}$$

and for a *2dof* system with $m1 = 200$ *kip-mass* and $m2 = 150$ *kip-mass*,

$$\begin{aligned} \textit{minimize} \quad & E[V_1^e] \\ \textit{over} \quad & k_1, k_2, c_1, c_2 \\ \textit{such that} \quad & y_1^e \leq 2 \ in \\ & y_2^e \leq 2 \ in \\ & c_1 + c_2 \leq 10 \ kip\_sec/in \\ & k_1 \geq 50 \ kip/in \\ & k_2 \geq 50 \ kip/in \end{aligned} \tag{3.44}$$

The solutions to these problems are presented in Table 3.4. Note that the *2dof* model utilizes all of the damping available while the *1dof* model rejects any damping beyond 39%. For the *1dof* model, the rejection of damping beyond certain values is clearly due to the increase in the intensity of acceleration response spectra at large damping and low frequencies. This phenomenon was discussed in Section 2.4.

3.8 Retrofitting a Building with a Soft First Story

A building with a soft first story is shown in Fig. 3.1. This is a common example in which, for space and aesthetic requirements, the unbraced columns in the first floor support the relatively rigid structure of the upper levels. In an intense earthquake plastic deformations concentrate in the soft story and ultimately cause the collapse of the entire structure (Arnold, 1989).

As an example consider the six-story building described in Section 1.3. Let the first floor columns be unbraced and constrained against rotation at both ends. Further assume that all other floors are adequately braced and thus comprise a rigid unit supported on the soft columns of the first floor. Under these circumstances the building can be modeled as a *1dof* system. For this model let a typical first floor

column have a lateral stiffness equal to 53 *kip/in*. The total weight of the rigid unit, corresponding to one column, is then equal to 300 *kips* — discounting the 50 *kips* weight of the base slab which is no longer required.

Table 3.4

Effect of damping

2dof system			*1dof system*		
units	*quantity*	*value*	*value*	*quantity*	*units*
kips	$E[V_1^e]$	68.3	78.2	$E[V^e]$	*kips*
kip/in	k_1	50	50	k	*kip/in*
kip/in	k_2	50	–	–	–
kip-sec/in	$c_1 + c_2$	10	5.30	c	*kip-sec/in*
kip-sec/in	c_1	6.15	–	–	–
kip-sec/in	c_2	3.85	–	–	–
in	y_1^e	1.5	1.7	y^e	*in*
in	y_2^e	0.9	–	–	–
g	$E[\ddot{x}_1^e]$	0.18	0.22	$E[\ddot{x}]$	*g*
g	$E[\ddot{x}_2^e]$	0.14	–	–	–
rad/sec	ω_1	16.5	7.4	$\bar{\omega}$	*rad/sec*
rad/sec	ω_2	6.8	–	–	–
–	ξ_1	0.73	0.39	ξ	–
–	ξ_2	0.38	–	–	–

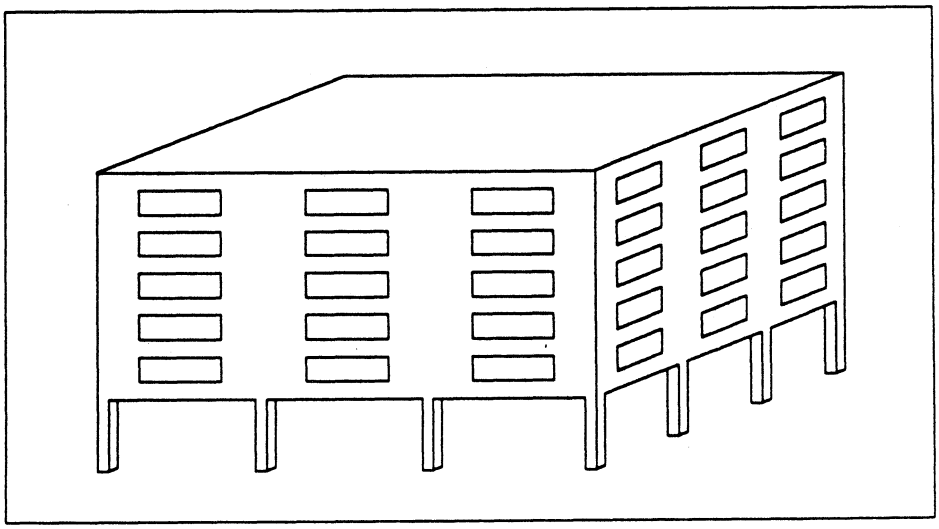

Fig. 3.1 *A rigid multistory building with a soft first story*

Based on an elastic design procedure, the allowable relative end displacement of the columns, due to the combined action of lateral motion and gravity loads, can be readily computed. In the example problem under consideration, a reasonable value for the allowable displacement is 0.45 *in*. This value, however, will be far exceeded in the event of a severe ground motion. To illustrate, the ground motion and the probabilistic method of analysis described earlier in Section 3.4 were used. The results for 5% damping, identified as case 1, are summarized in Table 3.5.

Table 3.5

Elastic solutions to the soft first story building example (using 1dof models)

units	*quantity*	*case 1*	*case 2*	*case 3*
kip-mass	m	300	300	300
kip/in	k	53	1171	609
kip-sec/in	c	0.59	3.02	8.7
rad/sec	$\bar{\omega}$	8.26	38.82	28.00
–	ξ	0.05	0.05	0.20
kips	$E[V^e]$	151.7	361.0	199.1
g	$E[\ddot{x}^e]$	0.51	1.20	0.66
in	y^e	4.68	0.45	0.45

Note that the relative column end displacement (4.68 *in*) is excessively large. In order to reduce this displacement to the allowable level at 0.45 *in*, the following options can be explored:

1. Provide adequate bracing in the first story.
2. Consider partial bracing in combination with supplemental damping devices in the first story.
3. Use the second option in conjunction with a modular scheme in which the roof or the top story are separated from the bottom portion by means of control elements.

These options can be studied in the context of the optimal design formulations presented in this chapter. For the first two options the following formulation can be

used:

$$\begin{aligned} \textit{minimize} \quad & E[V^e] \\ \textit{over} \quad & k, c \\ \textit{such that} \quad & y^e = 0.45\ in \\ & \xi \leq \xi^u \end{aligned} \tag{3.45}$$

in which ξ is the damping ratio as defined at the end of Section 3.2 and ξ^u is the upper bound on ξ. For the first option let $\xi^u = 5\%$ and for the second option, requiring supplemental mechanical dampers, use $\xi^u = 20\%$. The solutions are presented in Table 3.5 and are respectively identified as case 2 and case 3.

In case 2, large braces have to be used to provide the required lateral stiffness of 1171 *kip/in*. The acceleration in this case is also excessive (1.2 *g*), requiring strengthening of the upper stories. It should be noted that case 2 results are based on an *elastic* analysis. As such, these results do not reflect the forces and accelerations which will be obtained when retrofitting structures with braces that are allowed to yield and buckle consistent with a ductile design philosophy. The objective here is to obtain a retrofitting solution which guarantees elastic behavior. In this sense, case 3 provides a better solution because both the required lateral stiffness in the first story (609 *kip/in*) and the acceleration of the upper stories (0.66 *g*) are smaller.

Next consider the third option using the following minimization problem:

$$\begin{aligned} \textit{minimize} \quad & E[V_1^e] \\ \textit{over} \quad & k_1, k_2, c_1, c_2 \\ \textit{such that} \quad & y_1^e = 0.45\ in \\ & c_1 \leq 8.7\ kip\_sec/in \\ & c_2 \geq 0.1\ kip\_sec/in \end{aligned} \tag{3.46}$$

In this formulation, the upper bound on the first floor damping coefficient has been set equal to the damping required for the second option (case 3, Table 3.5). The solutions, for two different mass ratios, are provided in Table 3.6. Case 1 requires placement of the control elements under the roof while in case 2 the control elements are placed under the floor slab of the top story. With respect to the base shear, accelerations, and the lateral stiffness requirements in the first floor, both modular solutions in Table 3.6 indicate substantial advantages over those considered previously (Table 3.5). Again, tagging any one of the retrofitting options as the best solution requires at least a preliminary cost analysis.

Table 3.6

Elastic solutions to the soft first story building example (using 2dof modular models)

units	*quantity*	*case 1*	*case 2*
kip-mass	m_1	250	200
kip-mass	m_2	50	100
kip-mass	$m_1 + m_2$	300	300
kip/in	k_1	402	259
kip/in	k_2	16.2	9.4
kip-sec/in	c_1	8.7	8.7
kip-sec/in	c_2	1.1	1.5
rad/sec	ω_1	25.3	22.5
rad/sec	ω_2	11.0	6.0
–	ξ_1	0.31	0.44
–	ξ_2	0.36	0.46
kips	$E[V_1^e]$	119.2	84.7
g	$E[\ddot{x}_1^e]$	0.53	0.45
g	$E[\ddot{x}_2^e]$	0.41	0.22
in	y_1^e	0.45	0.45
in	y_2^e	1.37	1.46

CHAPTER 4

SUMMARY, CONCLUSIONS, AND FUTURE RESEARCH

4.1 Summary

The primary interest in this dissertation has been the optimum design of low to medium rise buildings subjected to intense earthquakes. In this regard the concept of modular structures was introduced. In its most general form a modular structure is composed of a stack of rigid stories or modules separated at their interface by passive control elements. These elements can be similar to currently used base isolation systems. They require a structural mechanism which is vertically stiff, laterally flexible, and provides some means of energy dissipation.

A modular structure can be described mathematically as a number of lumped masses consecutively connected by springs and dampers. In this model the lumped masses represent the rigid modules; and the springs and dampers represent the lateral mechanical properties of the control elements. The only control or design variables involved in the optimization of the response of such structures to earthquake excitation are the spring and damping coefficients of the control elements. These design variables can assume a wide range of values irrespective of the basic design requirements for gravity loads and interstory drift limits imposed on the modules. Consequently, a computationally manageable optimal design problem is facilitated.

Optimal design problems for structural vibrations are formulated based on the extreme values of the response quantities of interest. These extreme values can be obtained by a variety of methods which fall in the broad categories of the response spectrum approach, the time domain analysis, and the random vibration technique.

In the response spectrum approach the extreme values are obtained based on approximate modal combinations. In this case the structure must have proportional damping characteristics. In this research, both stiffness and damping coefficients were considered as variables of the optimal design problems. Therefore it was expected

that the damping coefficients would turn out to be nonproportional. Because of the damping proportionality restriction and the approximations involved in modal combinations, the response spectrum approach was not pursued in the investigation of the optimal designs.

The available time domain methods of optimal design require examination of the entire time history of a number of response quantities in an effort to reduce the extreme values of some while preventing others from exceeding certain admissible levels. It has been observed that the success of these methods depends on the character of excitation time history. In particular, single impulse excitations, for which the corresponding response spectra are smooth functions of frequency, can be effectively dealt with by these methods. An earthquake time history will however cause serious problems in the optimization process. The reason lies in the jaggedness of the earthquake response spectra; especially for lightly damped systems. In a mathematical search technique, at every advancement to an improved design point, a certain reduction in the objective function is sought without violating the constraints. Both the objective and constraints are functions of the extreme values of the response time histories. Since these quantities vary in a jagged pattern with respect to design variables, shortly after the initial point the search will halt at a locally ascending portion of the objective function or a slightly violated portion of the constraints. Although the point at which the optimization process is terminated qualifies as a local minimum, there are many other points in the design space with this same qualification. This is a serious drawback in terms of locating a global minimum by restarting the optimization at different initial points. Consequently, the time domain methods were not used in this research.

The aforementioned restrictions and shortcomings, associated with the response spectrum and time domain analyses, do not arise in the random vibration method. Therefore this method was selected for the optimal design investigations. The excitation and response relations were formulated in the frequency domain. This requires a knowledge of the power spectral density of the ground excitation process. The excitation process, used in the optimal design investigations, corresponds to a family of strong earthquake accelerations recorded on rock deposits in the vicinity of the source. Because the statistical characterizations of site-specific earthquakes are more widely available in the form of design response spectra, a new method was developed in this research to derive power spectral densities from design response spectra. In this effort an existing extreme value probability distribution, which has been shown to apply accurately to earthquake excitation and response processes, has been used

(Vanmarcke, 1975; Der Kiureghian, 1980b). Details of deriving power spectral densities from response spectra are presented in Sections 2.2 and 2.3. The highlights of the method are summarized in the following paragraph.

From the results obtained by Der Kiureghian (1980b), the expected extreme value of the acceleration of a single degree of freedom system, $E[\ddot{x}^e]$, can be written in terms of the transfer function associated with the acceleration of the mass, $Q_{\ddot{x}}$, and the power spectral density of the ground acceleration process, $S_{\ddot{x}_b}$:

$$E[\ddot{x}^e] = f\left(Q_{\ddot{x}}, S_{\ddot{x}_b}\right) \tag{4.1}$$

$Q_{\ddot{x}}$ is a function of the system frequency, $\bar{\omega}$, and the damping ratio, ξ. For a particular $\bar{\omega}$ and ξ, if $S_{\ddot{x}_b}$ is known (4.1) furnishes one point of a mean acceleration response spectrum. As mentioned previously, the interest is to derive $S_{\ddot{x}_b}$ from $E[\ddot{x}^e]$. Because an analytical inversion of (4.1), *i.e.* writing $S_{\ddot{x}_b}$ explicitly in terms of $E[\ddot{x}^e]$, is not possible, a computational inversion procedure was proposed. To this end, it was shown that (4.1) can be written in the following form:

$$S_{\ddot{x}_b} = \left(E[\ddot{x}^e]\right)^2 g\left(S_{\ddot{x}_b}\right) \tag{4.2}$$

where g is a known but complicated function of $S_{\ddot{x}_b}$. Based on an examination of the behavior of g, this function was approximated by a simple function of frequency, ω, and five unknown parameters, α_i $(i = 1, 2, 3, 4, 5)$. Denoting this function by h, (4.2) can be written as:

$$S_{\ddot{x}_b} = \left(E[\ddot{x}^e]\right)^2 h\left(\omega, \alpha_1, \alpha_2, \alpha_3, \alpha_4, \alpha_5\right) \tag{4.3}$$

In order to find the unknown parameters α_i, the following iterative procedure was used:

1. Start with a known mean acceleration response spectrum $E[\ddot{x}^e]$.
2. Guess initial values for parameters α_i.
3. Compute $S_{\ddot{x}_b}$ from (4.3).
4. Use $S_{\ddot{x}_b}$ just computed in (4.1) and evaluate $E[\ddot{x}^e]$.
5. If the newly computed $E[\ddot{x}^e]$ closely matches the known $E[\ddot{x}^e]$ in step 1, stop. Otherwise, continue.
6. Compute the function g in (4.2).

7. Compute new coefficients α_i based on least squares approximation of g by h at discrete values of ω.

8. Take the newly computed parameters α_i as the next guess and go to step 3.

It has been shown that this procedure produces acceptable results in a few iterations. A mean acceleration response spectrum with 5% damping, corresponding to strong earthquakes on rock deposits, was selected to obtain $S_{\ddot{x}_b}$. This spectral density was then used to generate response spectra for other damping ratios. It was shown that the resulting spectra closely match the actual response spectra with damping in the range of 5% to 20%.

Site-specific response spectra for damping ratios greater than 20% are not available. Therefore, for these high damping ratios, the validity of the derived excitation power spectral density was established qualitatively. As a result, it was observed that for the particular excitation process considered, the corresponding response spectra at frequencies below 15 *rad/sec* (periods above 0.4 *sec*) tend to increase as the damping ratios are increased beyond 40%. This same trend can also be observed in high damping response spectra computed for actual earthquake records (Ashour and Hanson, 1987). This observation implies that a low frequency oscillator, such as a base isolated structure, has an optimum value of damping.

Only one and two degree of freedom models were used in the optimal design investigations. These models represent a six-story building structure. The one degree of freedom model simulates the base isolated version of this structure; and the two degree of freedom model represents its various modular arrangements using two levels of control elements. In every modular case the first level of control elements was placed at the base, while the second level was placed at a higher location between adjacent stories or just under the roof.

For all models the optimal design problems were formulated as to minimize the base shear. The stiffness and damping coefficients of the control elements were considered as the design variables. The constraints included upper bounds on the lateral displacement and damping coefficients, and lower bounds on the stiffness of the control elements. The base shear was represented by its mean extreme value; while the displacements were written as the sum of their mean extreme value and a multiple four of the standard deviation of their extreme values. A computer program was written to solve these nonlinear optimization problems. The algorithm used is based on a well established gradient projection method due to Haug and Arora (1979).

The initial interest was to compare the performance of a one degree of freedom base isolated structure to that of a two degree of freedom modular structure. It is clear that the choice between base isolation and modular schemes should be based on either the most favorable response under equal resource availability; or the least resource consumption for the same level of response. Consequently, following the optimal design formulations, a discussion on the equivalence of resources used in each problem was presented. It was shown that a practically meaningful comparison requires a detailed cost analysis relative to each competing design option. Without access to actual cost data, a volumetric material analysis was conducted in the context of specific examples using laminated rubber bearings as the control elements.

Next, attention was turned to specific applications of a modular structure. In this regard two possibilities were explored. Firstly, the possibility of a desired response reduction by a modular structure with two levels of control elements was investigated. In this context, the benefits of large damping and vibration isolation in a modular structure were studied. Secondly, the effectiveness of a modular solution in retrofitting buildings with soft first stories were demonstrated.

4.2 Conclusions

The site-specific excitation process used in the optimal design investigations was selected to correspond to rock deposits. The dominant periods of this process are much shorter than the largest periods achievable in a base isolated structure. With this process, and the use of laminated rubber bearings as the control elements, the following conclusions were made:

1. The new method to derive power spectral densities from design response spectra is computationally simpler than other available methods.

   This method has been devised based on an existing extreme value probability distribution which has been shown to apply accurately to earthquake excitation and response processes.

2. For the same level of response to earthquakes on rock deposits, the construction of a base isolated building is less costly than that of a modular building.

   However, there are certain limitations associated with the feasibility of base isolation. Firstly, there are practical limits on the extent of flexibility and lateral displacement of a base isolation system. In such a situation a modular scheme can be viewed as a method of further response improvement without requiring

additional flexibility or displacement capacity at the base. Secondly, because of the practical limits just mentioned, base isolation is not a feasible option in protecting structures founded on soft soil deposits. Earthquakes recorded on soft soils, such as the ones in Mexico City, have dominant periods in the range of the longest periods that can be practically obtained with base isolation alone.

3. The modular system can provide an increase in the fundamental period of the building thereby providing a viable alternative for earthquake protection where base isolation is not satisfactory.

4. The modular scheme can be used to limit story shear forces and story displacements in existing seismically weak multistory structures.

   The application of the modular scheme to retrofitting existing multistory structures with soft and weak first stories was considered. The example required placement of one level of control elements under the roof or under the top floor slab. The characteristics of the control elements and the supplemental braces and dampers in the first story were established such that overall elastic behavior throughout the building was achieved during a severe earthquake. These results show that the proposed retrofitting solution can be effective and practical.

4.3 Future Research

The concept of a modular structure was introduced here for the first time and has been shown to have potential advantages in certain applications. The results warrant continued research to more fully establish the benefits of this concept. In this regard the following topics are recommended for future studies:

1. Investigate the cost effectiveness of modular structures using different types of control elements.

2. Study the applicability and practicality of modular structures with respect to earthquake characterizations on soft soil deposits.

3. Conduct studies with broader parameter variations for retrofitting solutions.

APPENDIX A

A NONLINEAR OPTIMIZATION PROGRAM

A.1 Introduction

Optimization software which are intended to solve nonlinear programming problems are commercially available (Haftka and Kamat, 1985). Successful implementation of a commercial optimization software for every problem is not however a simple task. Because of the nature of approximations inherent in optimization algorithms and the sensitivity of the related computational processes to the convergence tolerances and the program options, it is imperative that the user has a basic understanding of the underlying computational strategies employed. Beyond that, access to the source code or more preferably to the responsible party maintaining the software is of principal importance. In a situation where there is an abnormal halt in the solution process, any remedial attempt is certainly aided by knowing where in the algorithm the abnormality occurred and what the cause was.

In order to avoid potential difficulties in using a commercial program, a computer program was written based on a well established gradient projection method. The advantage of having one's own optimization program, in addition to its general usefulness, is the ease with which it can be manipulated in resolving potential problems that can occur during various computational processes.

This appendix provides a brief theoretical background leading to a computational algorithm which was used in the development of the computer program. For verification purposes, this program was used to solve several nonlinear programming problems with known solutions.

A.2 A Gradient Projection Method

The nonlinear design optimization problems encountered in this research can be cast in the following general form

$$\textit{minimize} \quad f(b) \tag{A.1}$$

$$\textit{such that} \quad h_i(b) \leq 0\,; \quad i = 1, ..., n \tag{A.2}$$

in which b is the vector of design variables; f is the objective function; and h_i represent n inequality constraints including upper and lower bounds on the design variables. The method of solution adopted here is based on a gradient projection technique with constraint compensation due to Haug and Arora (1979). In this method the objective and the active constraint functions are linearized at a given design vector b_0 from which an improved design vector b is sought such that the objective function is reduced while the active constraints remain feasible. This is accomplished through a move from b_0 in the projected direction of the steepest descent of the objective function onto the hyperplane defined by the gradients of active constraints. Since this move typically causes violation of some of the constraint functions, it is combined with a restoration move to compensate for the constraint violations. At every point thus obtained, the Kuhn-Tucker necessary conditions are invoked to check convergence of the objective function to a local minimum.

At a given feasible point b_0, the set of active constraints are identified as those h_i satisfying the following condition

$$-\epsilon \leq h_i(b_0) \leq 0\,; \quad i = 1, ..., n \tag{A.3}$$

in which ϵ is a small positive number. For convenience, let the active constraints be denoted as g_i. Thus

$$-\epsilon \leq g_i(b_0) \leq 0\,; \quad i = 1, ..., n_A \tag{A.4}$$

where $n_A < n$ is the total number of active constraints.

The advancement from b_0 to a new point b is obtained by choosing an incremental design vector δb such that the objective function is decreased while the active constraints are not violated. Mathematically, this requirement can be stated as

$$f(b) < f(b_0) \tag{A.5}$$

$$g_i(b) \leq 0\,; \qquad i = 1, ..., n_A \tag{A.6}$$

where

$$b = b_0 + \delta b \tag{A.7}$$

The incremental design vector δb must be small enough to allow representation of f and g_i, in the vicinity of b_0, by linear approximations. In this sense

$$f(b) = f(b_0) + \nabla f^T(b_0)\delta b \tag{A.8}$$

$$g_i(b) = g_i(b_0) + \nabla g_i^T(b_0)\delta b\,; \quad i = 1, ..., n_A \tag{A.9}$$

in which ∇ is the gradient operator; and the superscript T stands for the transpose. Within these linear approximations, satisfying the requirements (A.5) and (A.6) is equivalent to solving the following minimization problem at each iterate:

$$\textit{minimize} \quad \nabla f^T(b_0)\delta b \tag{A.10}$$

$$\textit{such that} \quad \nabla g_i^T(b_0)\delta b \leq -g_i(b_0)\,; \quad i = 1, ..., n_A \tag{A.11}$$

$$\delta b^T \delta b \leq \xi^2 \tag{A.12}$$

where ξ is a small positive number.

Under the assumption that the gradients of the active constraints ∇g_i, evaluated at b_0, are linearly independent, one can use the Kuhn-Tucker theorem to establish the necessary conditions for which δb is a local minimizer of the incremental minimization problem defined by (A.10) through (A.12). At a local minimum, the Kuhn-Tucker necessary conditions guarantee existence of n_A nonnegative multipliers μ_i, corresponding to (A.11), and a nonnegative multiplier γ, corresponding to (A.12), such that

$$\nabla f + \nabla g\mu + 2\gamma\delta b = 0 \tag{A.13}$$

$$\mu_i(\nabla g_i^T \delta b + g_i) = 0\,; \quad i = 1, ..., n_A \tag{A.14}$$

$$\gamma(\delta b^T \delta b - \xi^2) = 0 \tag{A.15}$$

in which

$$\nabla g\mu = \sum_{i=1}^{n_A} \mu_i \nabla g_i \tag{A.16}$$

The necessary conditions (A.13) to (A.15) are nonlinear in the unknowns δb, μ, and γ, causing difficulty in obtaining a solution. In order to circumvent this difficulty a strategy, as suggested by Haug and Arora (1979), is to assume

$$\nabla g_i^T \delta b = -g_i\,; \quad i = 1, ..., n_A \tag{A.17}$$

$$\delta b^T \delta b = \xi^2 \tag{A.18}$$

implying that the constraints (A.11) and (A.12) are tight, *i.e.* equal zero, and the multipliers μ_i and γ are nonnegative. Premultiplying (A.13) by ∇g^T leads to

$$\nabla g^T \nabla f + \nabla g^T \nabla g\mu + 2\gamma \nabla g^T \delta b = 0 \tag{A.19}$$

which, using (A.17), becomes

$$\nabla g^T \nabla f + \nabla g^T \nabla g \mu - 2\gamma g = 0 \tag{A.20}$$

From this equation the vector of multipliers μ can be evaluated in terms of the as yet unknown multiplier γ:

$$\mu = -(\nabla g^T \nabla g)^{-1} [\nabla g^T \nabla f - 2\gamma g] \tag{A.21}$$

Substituting μ from (A.21) into (A.13), the incremental design vector δb can be evaluated and written in the following form

$$\delta b = -\frac{1}{2\gamma} \delta b^I + \delta b^{II} \tag{A.22}$$

in which the components δb^I and δb^{II} are respectively given by

$$\delta b^I = [I - \nabla g (\nabla g^T \nabla g)^{-1} \nabla g^T] \nabla f \tag{A.23}$$

$$\delta b^{II} = -\nabla g (\nabla g^T \nabla g)^{-1} g \tag{A.24}$$

The quantity contained within the brackets in (A.23) is a symmetric positive definite projection matrix.

It is noted that once a value for γ is determined, both the multiplier vector μ and the incremental design vector δb become available through (A.21) and (A.22), respectively. A value for the multiplier γ can be established based on a certain desired reduction in the objective function at each iterate. Let δf, a positive number, denote the desired reduction. Therefore, as can be verified from (A.8), it is required that

$$\nabla f^T \delta b = -\delta f \tag{A.25}$$

As shown by Haug and Arora (1979), since it is the $-\frac{1}{2\gamma}\delta b^I$ component of δb which tends to reduce the objective function, (A.25) can be written in the following form

$$\nabla f^T (-\frac{1}{2\gamma} \delta b^I) = -\delta f \tag{A.26}$$

from which γ can be evaluated as

$$\gamma = \frac{\nabla f^T \delta b^I}{2\delta f} \tag{A.27}$$

The foregoing development has been based on the assumption that the multipliers μ_i and γ are all nonnegative. It is noted that γ as evaluated by (A.27) will always be nonnegative. The nonnegativity of the numerator in (A.27) can be established based

on the projection property of the matrix contained within the brackets in (A.23); and it was just mentioned that δf in the denominator is a selected positive number. As shown by Haug and Arora (1979), after computation of μ from (A.21), if any number of the multipliers μ_i turn out to be negative, it is an indication that the objective function can be further reduced by simply removing the corresponding constraints g_i from the active constraint set and repeating the iteration with the remaining active constraints.

Towards computational efficiency in evaluation of δb and μ, Haug and Arora (1979) decompose the vector μ in the form

$$\mu = \mu^I + 2\gamma\mu^{II} \tag{A.28}$$

in which μ^I and μ^{II} can be obtained from the following sets of linear equations:

$$(\nabla g^T \nabla g)\mu^I = -\nabla g^T \nabla f \tag{A.29}$$

$$(\nabla g^T \nabla g)\mu^{II} = g \tag{A.30}$$

With this arrangement, it can be verified that (A.23) and (A.24) can respectively be written as

$$\delta b^I = \nabla f + \nabla g \mu^I \tag{A.31}$$

$$\delta b^{II} = \nabla g \mu^{II} \tag{A.32}$$

Based on geometrical considerations pertaining to δb^I and δb^{II} , Haug and Arora (1979) have shown that as the solution of the original minimization problem, given by (A.1) and (A.2), is approached, δb^I approaches zero. This can be used as a stopping criteria in the following computational algorithm:

1. Guess an initial design b_0
2. Evaluate h_i at b_0 for $i = 1, ..., n$.
3. From an examination of h_i select the set of active constraints g_i, with indices i ranging consecutively from 1 to n_A, such that $-\epsilon \leq g_i \leq 0$ where ϵ is a small positive number such as 0.01.
4. Compute the gradient of the objective function ∇f evaluated at b_0
5. Compute the gradients of the active constraints ∇g_i evaluated at b_0 and form the matrix $\nabla g = [\nabla g_1 \ \nabla g_2 \ ... \ \nabla g_{n_A}]$

6. Compute μ^I from (A.29)

7. Compute δb^I from (A.31)

8. Choose a certain percentage reduction α in the objective function and evaluate $\delta f = \alpha f(b_0)$

9. Evaluate γ from (A.27)

10. Evaluate μ^{II} from (A.30) and Compute μ from (A.28). If any components of μ are negative, delete the corresponding constraints from the active set, reconstruct the matrix ∇g with the reduced number of active constraints and go to step 6. Otherwise continue.

11. Compute δb^{II} and form the new incremental design vector δb using (A.22)

12. Let $b_0 \leftarrow b_0 + \delta b$

13. Evaluate h_i at b_0 for $i = 1, ..., n$.

14. If all h_i are satisfied within an acceptable tolerance and $\delta b^{I^T} \delta b^I$ is small enough, terminate. Otherwise restart the iteration at step 3

A.3 Verification of the Computer Program

A Fortran computer program was written based on the computational algorithm presented in the preceding section. For verification purposes, this program was used to solve several nonlinear programming problems with known solutions. As an example, consider the following problem:

$$\begin{aligned} \textit{minimize} \quad & f(b) = 3b_1 + \sqrt{3}b_2 \\ \textit{such that} \quad & g_1(b) = -3 + \frac{18}{b_1} + \frac{6\sqrt{3}}{b_2} \leq 0 \\ & g_2(b) = -b_1 + 5.73 \leq 0 \\ & g_3(b) = -b_2 + 7.17 \leq 0 \end{aligned}$$

The program is started at the feasible point $b = (12, 12)$ at which

$$f = 56.78 \quad g_1 = -0.63 \quad g_2 = -6.27 \quad g_3 = -4.83$$

A 5% reduction in the objective function is sought with each descent move. The tolerance on constraint violations at the end of each descent move is set equal to 0.01.

This means that if the value of any one of the constraint functions evaluated at the end of a descent move exceeds .01, the percent reduction is decreased and the descent move repeated. The tolerance on the acceptability of a restoration move is set equal to 0.00001. This means that if at the end of a restoration move the violated constraints are not restored to within 0.00001 of the boundary of the feasible domain, then an additional restoration move is initiated. The tolerance on the stopping criteria is set equal to 0.01. With these parameters, the problem is solved after 24 iterations with the following results

$$b_1 = 9.455 \quad b_2 = 9.479 \quad f = 44.78 \quad \mu_1 = 14.87 \quad \mu_2 = 0 \quad \mu_3 = 0$$

Haftka and Kamat (1985) provide the following exact solution to the same minimization problem

$$b_1 = 9.464 \quad b_2 = 9.464 \quad f = 44.78 \quad \mu_1 = 14.93 \quad \mu_2 = 0 \quad \mu_3 = 0$$

Comparing the numerical and the exact solutions, it is concluded that the program produces acceptable results.

APPENDIX B

MODAL CHARACTER OF THE DESIGN PROBLEMS

B.1 Introduction

In a proportionally damped multiple degree of freedom structure, the modal damping ratios ξ_j provide means of assessing the amount of damping present in the system. The optimal design solutions in Chapter 3, which pertain to the two degree of freedom *(2dof)* modular models, all have nonproportional damping characteristics. Consequently, the usual definition of a modal damping ratio no longer applies to these problems.

In nonproportionally damped systems, some means of damping assessment is still desirable. The main purpose of this appendix is to provide the basis for an approximate evaluation of damping present in such systems.

B.2 Modal Characteristics

The homogeneous equilibrium equations of a linear multiple degree of freedom system can be represented in the following matrix form

$$M\ddot{u} + C\dot{u} + Ku = 0 \tag{B.1}$$

in which M is the mass matrix; C is the damping matrix; K is the stiffness matrix; and u, $\dot{u}$, and $\ddot{u}$ are, repectively, the displacement, velocity, and acceleration vectors. In the case of proportional damping, expansion of u in terms of the eigenvectors of the eigenvalue problem associated with the undamped version of (B.1), produces a set of uncoupled differential equations with modal frequencies ω_j and modal damping ratios ξ_j.

When C is nonproportional, a similar expansion procedure applies to a first order form of (B.1) from which the original solution u can be retrieved (Meirovitch, 1980). Addition of the identically zero system of equations

$$-K\dot{u} + K\dot{u} = 0$$

to (B.1) leads to the following first order form

$$\hat{M}\dot{v} + \hat{K}v = 0 \tag{B.2}$$

in which the vectors v and $\dot{v}$ are represented by

$$v = \begin{Bmatrix} \dot{u} \\ u \end{Bmatrix} \; ; \quad \dot{v} = \begin{Bmatrix} \ddot{u} \\ \dot{u} \end{Bmatrix} \tag{B.3}$$

and the partitioned matrices $\hat{M}$ and $\hat{K}$ are defined as

$$\hat{M} = \begin{bmatrix} M & 0 \\ 0 & -K \end{bmatrix} \; ; \quad \hat{K} = \begin{bmatrix} C & K \\ K & 0 \end{bmatrix} \tag{B.4}$$

Substitution of a solution of the form

$$v = \varphi e^{\lambda t}$$

in (B.2) leads to the following eigenvalue problem

$$A\varphi = \lambda\varphi \tag{B.5}$$

in which

$$A = -\hat{M}^{-1}\hat{K} = \begin{bmatrix} -M^{-1}C & M^{-1}K \\ I & 0 \end{bmatrix} \tag{B.6}$$

The eigenvectors φ_j and eigenvalues λ_j of problem (B.5) are in general complex and appear in conjugate pairs. For stable dynamical systems, λ_j will have negative real parts; and those in the upper complex half plane can be represented as

$$\lambda_j = -\zeta_j + i\theta_j \tag{B.7}$$

in which $i = \sqrt{-1}$; and both components ζ_j and θ_j are positive.

In the case of *proportional* damping, the eigenvalues λ_j can be written in terms of the modal frequencies ω_j and modal damping ratios ξ_j; thus

$$\lambda_j = -\xi_j\omega_j + i\omega_j\sqrt{1-\xi_j^2} \tag{B.8}$$

Comparison of (B.7) and (B.8) shows that, when damping is proportional, θ_j is equal to the j^{th} damped modal frequency while ζ_j is a measure of the decay rate of the j^{th} modal response. From (B.7) and (B.8) it follows that

$$\omega_j = \sqrt{\zeta_j^2 + \theta_j^2} \tag{B.9}$$

$$\xi_j = \frac{\zeta_j}{\sqrt{\zeta_j^2 + \theta_j^2}} \tag{B.10}$$

Although (B.9) and (B.10) are exact for the proportional damping case only, they can be viewed as approximate relations in the case of nonproportional damping (Minami, 1977).

The optimal design solutions to the *2dof* modular models in Chapter 3, all turn out to have nonproportional damping. The frequencies ω_j and damping ratios ξ_j for these problems have been computed from the relations (B.9) and (B.10). Using the assumptions and notations employed in Section 3.3, the matrices M, C, and K of a *2dof* modular model take the following forms

$$M = \begin{bmatrix} m_1 & 0 \\ 0 & m_2 \end{bmatrix} \; ; \quad C = \begin{bmatrix} c_1 + c_2 & -c_2 \\ -c_2 & c_2 \end{bmatrix} \; ; \quad K = \begin{bmatrix} k_1 + k_2 & -k_2 \\ -k_2 & k_2 \end{bmatrix}$$

from which the matrix A as given by (B.6) is readily constructed. The eigenvalues of A can be extracted using commercially available computer programs.

As an example consider the *2dof* system in Table 3.1. The mass, damping, and stiffness properties of this system are

$$\begin{aligned} m_1 &= 300 \quad kip\_mass \; ; \; c_1 = 0.046 \quad kip\_sec/in \; ; \; k_1 = 30.73 \quad kip/in \\ m_2 &= 50 \quad kip\_mass \; ; \; c_2 = 0.319 \quad kip\_sec/in \; ; \; k_2 = 3.58 \quad kip/in \end{aligned}$$

With these numerical values, the eigenvalues λ_j are computed as

$$\begin{aligned} \lambda_1 &= -0.808 + i6.741 \\ \lambda_2 &= -0.659 + i4.825 \end{aligned}$$

Subsequently, the frequencies and damping ratios can be evaluated using (B.9) and (B.10):

$$\begin{aligned} \omega_1 &= 6.79 \quad rad/sec \; ; \; \xi_1 = 0.12 \\ \omega_2 &= 4.87 \quad rad/sec \; ; \; \xi_2 = 0.14 \end{aligned}$$

APPENDIX C

LIST OF SYMBOLS

C.1 Symbols in Chapter 1

$\downarrow$	a decrease in the adjacent quantity
$\uparrow$	an increase in the adjacent quantity
1dof	one degree of freedom
2dof	two degree of freedom
α	a positive constant
β	allowable shearing strain of rubber
δ	lateral displacement of a laminated rubber bearing
$\bar{\omega}$	circular frequency of a one degree of freedom system
d	spectral displacement
E	modulus of elasticity
ft^2	square foot
G	shear modulus of rubber
h	$h_r + h_s$
h_r	thickness of a rubber layer in a laminated rubber bearing
h_s	thickness of a steel layer in a laminated rubber bearing
I	moment of inertia of a column cross section
k	stiffness coefficient in a *1dof* base isolated model
k_0	stiffness
k_1	stiffness
$\hat{k}_0$	stiffness corresponding to a local minimum reached from k_0
$\hat{k}_1$	stiffness corresponding to a local minimum reached from k_1
$k^\star$	stiffness corresponding to the global minimum
kips	kilo-pounds
$\bar{K}_l$	lateral stiffness of a circular rubber layer constrained between two stiff

	plates
$\bar{K}_t$	tilting stiffness of a circular rubber layer constrained between two stiff plates
$\bar{K}_v$	vertical stiffness of a circular rubber layer constrained between two stiff plates
K_l	lateral stiffness of a circular rubber bearing
K_t	tilting stiffness of a circular rubber bearing
K_v	vertical stiffness of a circular rubber bearing
L	total length of a laminated rubber bearing
n	number of rubber layers in a laminated rubber bearing
P	axial force
P_c	critical buckling load of a laminated rubber bearing
psd	power spectral density
psf	pounds per square foot
psi	pounds per square inch
q	quantity as defined by equation (1.5)
R	radius of a circular rubber bearing
S	shear force
W_1	weight below the second level of control elements
W_2	weight above the second level of control elements
M	mass

C.2 Symbols in Chapter 2

α	a positive constant which appears in equations (2.19) and (2.21)
β	allowable shearing strain of rubber
δ	lateral displacement of a laminated rubber bearing
λ_0	first spectral moment of the random process z defined by equation (2.2)
λ_1	second spectral moment of the random process z defined by equation (2.2)
λ_2	third spectral moment of the random process z defined by equation (2.2)
ν	spectral parameter as defined by equation (2.4)
ν_0	spectral parameter as defined by equation (2.8)
ξ	damping ratio of a one degree of freedom system
ξ_g	damping ratio of the ground modeled as a single degree of freedom system
ϕ	function as defined by equation (2.17)

ψ function defined by equations (2.19) or (2.21)

σ_{z^e} standard deviation of the random variable z^e

τ duration

ω circular frequency

ω_0 a constant circular frequency

$\bar{\omega}$ circular frequency of a one degree of freedom system

ω_g circular frequency of the ground modeled as a one degree of freedom system

b_1 a constant which appears in equation (2.17)

b_2 a constant which appears in equation (2.17)

c_1 a constant which appears in equation (2.17)

c_2 a constant which appears in equation (2.17)

$E[\ddot{x}^e]$ mean or expected value of the random variable $\ddot{x}^e$

$E[z^e]$ mean or expected value of the random variable z^e

exp exponential function

g gravitational acceleration equal to 386.088 in/sec^2

$H_{\ddot{x}}$ complex frequency response associated with the random process $\ddot{x}$

H_z complex frequency response associated with the random process z

i imaginary number defined as $\sqrt{-1}$

in inches

km kilometers

ln natural logarithmic function

P probability distribution function

p function defined by equation (2.10)

psd power spectral density

Q_z transfer function associated with the random process z

q spectral parameter as defined be equation (2.5)

R radius of a circular laminated rubber bearing

r normalized barrier level defined by $z_0/\sqrt{\lambda_0}$

rad radians

S_0 intensity of a constant power spectral density

S_z power spectral density of the random process z

$S_{\ddot{x}_b}$ power spectral density of the ground acceleration process $\ddot{x}_b$

sec seconds

t_f the first time at which z crosses z_0 (first passage time)

x absolute displacement of a one degree of freedom system

$\dot{x}$ absolute velocity of a one degree of freedom system

$\ddot{x}$ absolute acceleration of a one degree of freedom system

$\ddot{x}^e$ a random variable signifying the extreme values of the random process $\ddot{x}$

$\ddot{x}_b$ absolute acceleration of the ground

z a general response process

z_0 a constant barrier level on the random process z

z^e a random variable signifying the extreme values of the random process z

C.3 Symbols in Chapter 3

1dof one degree of freedom

2dof two degree of freedom

β a nonnegative number set equal to 4 in all examples

Δ quantity defined by equation (3.19)

δ lateral displacement of a laminated rubber bearing

ξ damping ratio of a *1dof* base isolated model

ξ_j modal damping ratio as defined in Appendix B

σ_{y^e} standard deviation of the random variable y^e

$\sigma_{y_1^e}$ standard deviation of the random variable y_1^e

$\sigma_{y_2^e}$ standard deviation of the random variable y_2^e

σ_{z^e} standard deviation of the random variable z^e

ω circular frequency

$\bar{\omega}$ circular frequency of a *1dof* base isolated model

ω_j modal frequency as defined in Appendix B

c damping coefficient of the control elements in a *1dof* base isolated model

c^u upper bound on c

c_1 damping coefficient of the first level of control elements in a *2dof* modular model

c_1^u upper bound on c_1

c_2 damping coefficient of the second level of control elements in a *2dof* modular model

c_2^u upper bound on c_2

$E[\ddot{x}^e]$ mean or expected value of the random variable $\ddot{x}^e$

$E[z^e]$ mean or expected value of the random variable z^e

exp exponential function

ft^3 cubic foot

G	shear modulus of rubber
g	gravitational acceleration equal to 386.088 in/sec^2
$H_{\ddot{x}}$	complex frequency response associated with $\ddot{x}$
$H_{\ddot{x}_1}$	complex frequency response associated with $\ddot{x}_1$
$H_{\ddot{x}_2}$	complex frequency response associated with $\ddot{x}_2$
H_y	complex frequency response associated with y
H_{y_1}	complex frequency response associated with y_1
H_{y_2}	complex frequency response associated with y_2
H_V	complex frequency response associated with V
H_{V_1}	complex frequency response associated with V_1
H_{V_2}	complex frequency response associated with V_2
H_z	complex frequency response associated with z
h_r	thickness of a rubber layer in a laminated rubber bearing
i	imaginary number defined as $\sqrt{-1}$
in	inches
K_l	lateral stiffness of a circular rubber bearing
K_v	vertical stiffness of a circular rubber bearing
k	lateral stiffness of the control elements in a *1dof* base isolated
k^l	lower bound on k
k_1	lateral stiffness of the first level of control elements in a *2dof* modular model
k_1^l	lower bound on k_1
k_2	lateral stiffness of the second level of control elements in a *2dof* modular model
k_2^l	lower bound on k_2
kip	kilo-pound
kips	kilo-pounds
km	kilometers
m	mass of a *1dof* base isolated model
m_1	mass of the module above the base in a *2dof* modular model
m_2	mass of the module above m_1 in a *2dof* modular model
n	number of rubber layers in a laminated rubber bearing
P	probability distribution function
P_c	critical buckling load of a laminated rubber bearing
psd	power spectral density
psi	pounds per square inch

R radius of a circular rubber bearing

rad radians

$S_{\ddot{x}_b}$ power spectral density of the ground acceleration process $\ddot{x}_b$

sec seconds

t time

V base shear in a *1dof* base isolated model defined as $c\dot{y} + ky$

V_1 base shear in a *2dof* modular model defined as $c_1\dot{y}_1 + k_1 y_1$

V_2 shear at the second level of control elements in a *2dof* modular model defined as $c_2\dot{y}_2 + k_2 y_2$

vol_r volume of rubber used in a laminated rubber bearing

vol_s volume of steel used in a laminated rubber bearing

x absolute displacement of m in a *1dof* base isolated model

x_1 absolute displacement of m_1 in a *2dof* modular model

x_2 absolute displacement of m_2 in a *2dof* modular model

x_b absolute displacement of the ground

$\dot{x}$ absolute velocity of m in a *1dof* base isolated model

$\dot{x}_1$ absolute velocity of m_1 in a *2dof* modular model

$\dot{x}_2$ absolute velocity of m_2 in a *2dof* modular model

$\ddot{x}$ absolute acceleration of m in a *1dof* base isolated model

$\ddot{x}_1$ absolute acceleration of m_1 in a *2dof* modular model

$\ddot{x}_2$ absolute acceleration of m_2 in a *2dof* modular model

$\dot{x}_b$ absolute velocity of the ground

$\ddot{x}_b$ absolute acceleration of the ground

y relative displacement of m in a *1dof* system defined as $x - x_b$

y^e extreme value of y defined as $E[y^e] + \beta\sigma_{y^e}$

y^u upper bound on y^e

y_1 relative displacement of m_1 in a *2dof* modular model defined as $x_1 - x_b$

y_1^e extreme value of y_1 defined as $E[y_1^e] + \beta\sigma_{y_1^e}$

y_1^u upper bound on y_1^e

y_2 relative displacement of m_2 in a *2dof* modular model defined as $x_2 - x_1$

y_2^e extreme value of y_2 defined as $E[y_2^e] + \beta\sigma_{y_2^e}$

y_2^u upper bound on y_2^e

$\dot{y}$ relative velocity of m in a *1dof* base isolated model defined as $\dot{x} - \dot{x}_b$

$\dot{y}_1$ relative velocity of m_1 in a *2dof* modular model defined as $\dot{x}_1 - \dot{x}_b$

$\dot{y}_2$ relative velocity of m_2 in a *2dof* modular model defined as $\dot{x}_2 - \dot{x}_1$

$\ddot{y}$ relative acceleration of m in a *1dof* base isolated model defined as $\ddot{x} - \ddot{x}_b$

$\ddot{y}_1$ relative acceleration of m_1 in a *2dof* modular model defined as $\ddot{x}_1 - \ddot{x}_b$

$\ddot{y}_2$ relative acceleration of m_2 in a *2dof* modular model defined as $\ddot{x}_2 - \ddot{x}_1$

z a general response process

z_0 a constant barrier level on the random process z

z^e a random variable signifying the extreme values of the random process z

C.4 Symbols in Chapter 4

α_i constants

ξ damping ratio of a one degree of freedom system

ω circular frequency

$\bar{\omega}$ circular frequency of a one degree of freedom system

$E[\ddot{x}^e]$ mean or expected value of the random variable $\ddot{x}^e$

f function

g function

h function

$Q_{\ddot{x}}$ transfer function associated with the random process $\ddot{x}$

$S_{\ddot{x}_b}$ power spectral density of the ground acceleration process $\ddot{x}_b$

$\ddot{x}$ absolute acceleration of a one degree of freedom system

$\ddot{x}^e$ a random variable signifying the extreme values of the random process $\ddot{x}$

$\ddot{x}_b$ absolute acceleration of the ground

C.5 Symbols in Appendix A

-1 used as a superscript to signify the inverse of a matrix

∇ the gradient operator

∇f the gradient of f

∇g the matrix of vectors ∇g_i defined as $[\nabla g_1 \ \nabla g_2 \ ... \ \nabla g_{n_A}]$

∇g_i the gradient of g_i

α percentage reduction in the objective function f

γ lagrangian multiplier

δb incremental design vector

δb^I component of δb

δb^{II} component of δb

δf desired reduction in objective function f — a small positive number

ϵ a small positive number

μ vector of lagrangian multipliers μ_i, $i = 1, 2, ..., n_A$

μ^I component of μ

μ^{II} component of μ

μ_i the i^{th} component of μ

ξ a small positive number

b vector of design variables b_j, $j = 1, 2, ..., m$

b_j the j^{th} component of b

b_0 a given design vector b

f objective function — a function of b

g the vector of active constraint functions g_i

g_i the i^{th} active constraint function; $i = 1, 2, ..., n_A$

h_i the i^{th} constraint function; $i = 1, 2, ..., n$

m maximum number of design variables

n maximum number of constraint functions h_i

n_A maximum number of active constraint functions g_i

T used as superscript to signify the transpose of a vector or a matrix

C.6 Symbols in Appendix B

-1 used as a superscript to signify the inverse of a matrix

0 zero, a zero vector, or a zero matrix as applicable

2dof two degree of freedom

ζ_j real part of λ_j

θ_j imaginary part of λ_j

λ_j j^{th} eigenvalue associated with φ_j

ξ_j j^{th} modal damping ratio as defined by equation (B.10)

φ eigenvector

φ_j j^{th} eigenvector

ω_j j^{th} modal frequency as defined by equation (B.9)

A matrix as defined by equation (B.6)

C damping matrix

c_1 damping coefficient of the first level of control elements in a *2dof* modul model

c_2 damping coefficient of the second level of control elements in a *2dof* modular model

I identity matrix

i imaginary number equal to $\sqrt{-1}$

in inches

K stiffness matrix

$\hat{K}$ matrix as defined by equation (B.4)

k_1 lateral stiffness of the first level of control elements in a *2dof* modular model

k_2 lateral stiffness of the second level of control elements in a *2dof* modular model

kip kilo pounds

M mass matrix

$\hat{M}$ matrix as defined by equation (B.4)

m_1 mass of the module above the base in a *2dof* modular model

m_2 mass of the module above m_1 in a *2dof* modular model

rad radians

sec seconds

t time

u displacement vector

$\dot{u}$ velocity vector

$\ddot{u}$ acceleration vector

v vector as defined by equation (B.3)

$\dot{v}$ vector as defined by equation (B.3)

REFERENCES

Arnold, C. (1989), "Architectural Considerations," *The Seismic Design Handbook,* Chapter 5, Edited By F. Naeim, Van Nostrand Reinhold, New York.

Ashour, S. A., and Hanson, R. D. (1987), "Elastic Seismic Response of Buildings with Supplemental Damping," *UMCE 87-1,* The University of Michigan, Department of Civil Engineering, Ann Arbor, Michigan.

Berg, G. V. (1989), *Elements of Structural Dynamics,* Prentice Hall, Englewood Cliffs, New Jersey.

Bergman, D. M., and Hanson, R. D. (1988), "Characteristics of Mechanical Dampers," *Proceedings of Ninth World Conference on Earthquake Engineering,* Japan, Vol. 5, pp. 815-820.

BSSC (1988), *NEHRP Recommended Provisions for the Development of Seismic Regulations for New Buildings,* Building Seismic Safety Council, Washington, D. C.

Chalhoub, M. S., and Kelly, J. M. (1990), "Effect of Bulk Compressibility on the Stiffness of Cylindrical Base Isolation Bearings," *International Journal of Solids and Structures,* Vol. 26, No. 7, pp. 743-760.

Clough, R. W., and Mojtahedi, S. (1976), "Earthquake Response Analysis Considering Nonproportional Damping," *Earthquake Engineering and Structural Dynamics,* Vol. 4, pp. 489-496.

Crandall, S. H., and Mark, W. D. (1963), *Random Vibration in Mechanical Systems,* Academic Press, Inc., Orlando, Florida.

Curtis, A. J., and Boykin, Jr., T. R. (1961), "Response of Two Degree of Freedom Systems to White Noise Base Excitation," *Journal of the Acoustical Society of America,* Vol. 33, No. 5, pp. 655-663.

Der Kiureghian, A. (1980a), "Probabilistic Modal Combination for Earthquake Loading," *Proceedings of seventh World Conference on Earthquake Engineering,* Istanbul, Turkey, Vol. 6, pp. 729-736.

Der Kiureghian, A. (1980b), "Structural Response to Stationary Excitation," *Journal of the Engineering Mechanics Division,* ASCE, Vol. 106, No. EM6, pp. 1195-1213.

Derham, C. J., and Thomas, A. G. (1983), "The Stability of Rubber/Steel Laminated Building Bearings," *NR Technology,* Vol. 14, Part 3, Publication 1006, pp. 52-58.

Gasparini, D., and Vanmarcke, E. H. (1976), "Simulated Earthquake Motions Compatible with Prescribed Response Spectra," MIT, Publication No. R76-4, Cambridge, Massachusetts.

Gent, A. N. (1964), "Elastic Stability of Rubber Compression Springs," *Journal of Mechanical Engineering Science,* Vol. 6, No. 4, pp. 318-326.

Gent, A. N., and Meinecke, E. A. (1970), "Compression, Bending, and Shear of Bonded Rubber Blocks," *Polymer Engineering and Science,* Vol. 10, No. 1, pp. 48-53.

Haftka, R. T., and Kamat, M. P. (1985), *Elements of Structural Optimization,* Martinus Nijhoff Publishers, Dordrecht, The Netherlands.

Haringx, J. A. (1948), "On Highly Compressible Helical Springs and Rubber Rods and their Applications for Vibration-Free Mountings, I," *Philips Research Reports,* Vol. 3, NR 6, pp. 401-449.

Haug, E. J., and Arora, J. S. (1979), *Applied Optimal Design,* John Wiley & Sons, Inc., New York.

Herrmann, L. R., Ramaswamy, A., and Hamidi, R. (1989), "Analytical Parameter Study for Class of Elastomeric Bearings," *Journal of Structural Engineering,* ASCE, Vol. 115, No. 10, pp. 2415-2434.

Kanai, K. (1957), "Semi-empirical Formula for the Seismic Characteristics of the Ground," *Bulletin of Earthquake Research Institute,* Japan, Vol. 35, pp. 309-325.

Kaynia, A. M., Veneziano, D., and Biggs J. M. (1981), "Seismic Effectiveness of Tuned Mass Dampers," *Journal of the Structural Division,* ASCE, Vol. 107, No. ST8, pp. 1465-1484.

Kelly, J. M. (1986), "Progress and Prospects in Base Isolation," *ATC-17, Proceedings of a Seminar and Workshop on Base Isolation and Passive Energy Dissipation,* Applied Technology Council, San Francisco, California, pp. 29-37.

Kelly, J. M., and Beucke, K. E. (1983), "A Friction Damped Base Isolation System with Fail-Safe Characteristics," *Earthquake Engineering and Structural Dynamics,* Vol. 11, pp. 33-56.

Kelly, J. M., and Skinner, M. S. (1979), "A Review of Current Uses of Energy Absorbing Devices," *EERC Report 79-10,* University of California, Berkley.

Lai, S. P. (1982), "Statistical Characterization of Strong Ground Motions Using Power Spectral Density Functions," *Bulletin of the Seismological Society of America,* Vol. 72, No. 1, pp. 259-274.

Lin, B. C., Tadjbakhsh, I. G., Papageorgiou, A. S., and Ahmadi, G. (1990), "Performance of Earthquake Isolation Systems," *Journal of Engineering Mechanics,* ASCE, Vol. 116, No. 2, pp. 446-461.

Mayes, R. L. (1989), "Design of Structures with Seismic Isolation," *The Seismic Design Handbook,* Chapter 13, Edited By F. Naeim, Van Nostrand Reinhold, New York.

McNamara, R. J. (1977), "Tuned Mass Dampers for Buildings," *Journal of the Structural Division,* ASCE, Vol. 103, No. ST9, pp. 1785-1798.

Meirovitch, L. (1980), *Computational Methods in Structural Dynamics,* Sijthoff and Noordhoff, Rockville, Maryland.

Minami, J. K., and Sakurai, J. (1977), "Earthquake Resistant Design of Buildings Considering Soil Types and Foundation Construction," *Memoirs of the School of Science and Engineering,* No. 41, Waseda University, Tokyo, Japan, pp. 1-30.

Mohraz, B. (1976), "A Study of Earthquake Response Spectra for Different Geological Conditions," *Bulletin of the Seismological Society of America,* Vol. 66, No. 3, pp. 915-935.

Mohraz, B., and Elghadamsi, F. E. (1989), "Earthquake Ground Motion and Response Spectra," *The Seismic Design Handbook,* Chapter 2, Edited By F. Naeim, Van Nostrand Reinhold, New York.

Mokha, A., and Constantinou, M. (1990), "Teflon Bearings in Base Isolation, I: Testing," *Journal of Structural Engineering,* ASCE, Vol. 116, No. 2, pp. 438-454.

Newmark, N. M., and Rosenblueth, E. (1971), *Fundamentals of Earthquake Engineering,* Prentice-Hall, Inc., New Jersy.

Nigam, N. C. (1983), *Introduction to Random Vibrations,* MIT press, Cambridge, Massachusetts.

Pfaffinger, D. D. (1983), "Calculation of Power Spectra from Response Spectra," *Journal of the Engineering Mechanics Division,* ASCE, Vol. 109, No. 1, pp. 357-372.

Roeder, C. W., and Stanton, J. F. (1983), "Elastomeric Bearings: State-of-the-Art," *Journal of Structural Engineering,* ASCE, Vol. 109, No. 12, pp. 2853-2871.

Roeder, C. W., Stanton, J. F., and Taylor, A. W. (1987), "Performance of Elastomeric Bearings," *National Cooperative Highway Research Program Report,* No. 248, Transportation Research Board, National Research Council, Washington, D.C.

Scanlan, R. H., and Sachs, K. (1974), "Earthquake Time Histories and Response Spectra," *Journal of the Engineering Mechanics Division,* ASCE, Vol. 100, No. EM4, pp. 635-655.

Seed, H. B., Ugas, C., and Lysmer, J. (1976), "Site Dependent Spectra for Earthquake Resistant Design," *Bulletin of the Seismological Society of America,* Vol. 66, No. 1, pp. 221-243.

Slasek, J. R., and Klingner, R. E. (1983), "Effect of Tuned-Mass Dampers on Seismic Response," *Journal of Structural Engineering,* ASCE, Vol. 109, No. 8, pp. 2004-2009.

Tajimi, H. (1960), "A Statistical Method of Determining the Maximum Response of a Building Structure During an Earthquake," *Proceedings of Second World Conference on Earthquake Engineering,* Japan, pp. 781-797.

Tanabashi, R. (1960), "Earthquake Resistance of the Traditional Japanese Wooden Structures," *Proceedings of Second World Conference on Earthquake Engineering,* Japan, pp. 151-163.

Vanmarcke, E. H. (1975), "On the Distribution of the First Passage Time for Normal Stationary Random Processes," *Journal of Applied Mechanics,* ASME, Vol. 42, pp. 215-220.

Wilson, E. L., Der Kiureghian, A., and Bayo, E. P. (1981), "A Replacement for the SRSS Method in Seismic Analysis," *Earthquake Engineering and Structural Dynamics,* Vol. 9, pp. 187-194.